QUANTIFYING THE PROTONOSPHERIC
EFFECT ON PRISM

THESIS

Kelly B. Doser, Captain, USAF

AFIT/GAP/ENP/00M-02

DEPARTMENT OF THE AIR FORCE
AIR UNIVERSITY

AIR FORCE INSTITUTE OF TECHNOLOGY

Wright-Patterson Air Force Base, Ohio

20001113 033

QUANTIFYING THE PROTONOSPHERIC
EFFECT ON PRISM

THESIS

Kelly B. Doser, Captain, USAF

AFIT/GAP/ENP/00M-02

QUANTIFYING THE PROTONOSPHERIC
EFFECT ON PRISM

THESIS

Presented to the Faculty

Department of Engineering Physics

Graduate School of Engineering and Management

Air Force Institute of Technology

Air University

Air Education and Training Command

In Partial Fulfillment of the Requirements for the Degree of

Master of Science in Physics
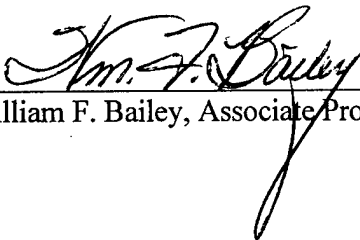
Kelly B. Doser, B.S.E.E., B.S.
Captain, USAF

March 2000

QUANTIFYING THE PROTONOSPHERIC
EFFECT ON PRISM

Kelly B. Doser, A.E.T., B.S.E.E., B.S.
Captain, USAF

Approved:

_____   _____
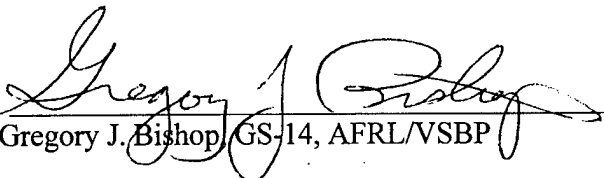William F. Bailey, Associate Professor (Chairman)   date
                                                                            2 Mar 00

_____   _____
Devin J. Della-Rose, Maj, USAF   date
                                                                            2 Mar 00

_____   _____
Gregory J. Bishop, GS-14, AFRL/VSBP   date
                                                                            11 Feb 2000

<u>Table of Contents</u>

List of Tables

Abstract

The total electron content (TEC) contribution to a Parameterized Real-time Ionospheric Specification Model (PRISM) calculation has been studied using protonospheric TEC measurements made by Global Positioning Satellites (GPS). Including the protonosphere proved challenging to both the calibration of GPS measurements and execution of PRISM. Though 46 days of GPS measurements were acquired, only 40 were successfully calibrated, and only 35 of those were used in the study. Data issues such as availability and completeness as well as measurement quality affected 6 of the days used. Calibration was done at Pittsburgh by excluding all measurements below 40.75° N. latitude cutoff. This latitude produced a plasmaspheric contribution to GPS TEC of 2.5 – 3.0 TEC units (TECu). Five calibrated days were collected during geomagnetic storm and recovery days, and could not be used in PRISM, reducing the data set to 35 days. Throughout the data, GPS trajectories added up to 3 TECu of error due to low elevation angles and multipath affects. PRISM was found to model the ionosphere with 10.4% to 17% average error, and included a protonospheric contribution result of 1.0 TECu. GPS measurement errors on the order of 3.0 TECu overwhelmed the 17% errors found in PRISM under the same conditions. During quiet periods, the model worked well, with most of the error coming from the GPS TEC measurements.

1. Introduction

Problem Statement

Our ability to accurately model the ionosphere has improved steadily over the years, but still falls short of the resolutions needed to specify the region particularly during periods of ionospheric disturbance. Addressing the ionic content at altitudes above what is historically considered the ionosphere is a critical difficulty. Altitudes above approximately 1600 km, known as the plasmasphere, also have ionic content, and can actually account for up to 50% of a total electron content (TEC) measurement [Lunt et al., 1999]. Recent efforts to tackle this problem include the addition of the Gallagher empirical protonospheric model in the Parameterized Real-time Ionospheric Specification Model (PRISM), and the planned expansion of PRISM to model beyond the 1600 km. Many studies assessed PRISM's ability to represent the structure of the ionosphere [Daniell et al., 1995, Coxwell, 1996, Filby, 1997]. What remains to be answered is, what's the quantifiable effect of the protonospheric distortion on PRISM? And this question really involves two parts, both the effect of the protonosphere in the input data driver for PRISM and the errors in slant TEC calculated by PRISM (for regions of the sky where there is a protonospheric contribution).

Motivation

1.1.1. Military Need

Specifying and forecasting densities in the ionosphere is an important factor in several aspects of military and civilian communications and space operations. Nearly all forms of long-range radio-wave propagation are directly affected by the presence of electrons in the ionosphere. Of particular interest are satellite communication and navigational signals

which are directly affected by the presence of ionosphere. Accurate, global, and timely specification and forecasting of the ionosphere could provide not only the tools needed to maintain proper communications and operations during times of ionospheric disturbances, but could also provide the informed user a military intelligence advantage.

1.1.2. Why Care About Protonosphere (Plasmasphere)?

Figure 1 shows the protonosphere is a co-rotational toroidal shaped plasma region extending from the transition region of the ionosphere to 30,000 km (or 4 Earth Radii, 4 R_e) at the magnetic equator, and terminating at the top of the ionosphere at approximately $\pm 60^{\circ}$ latitude.
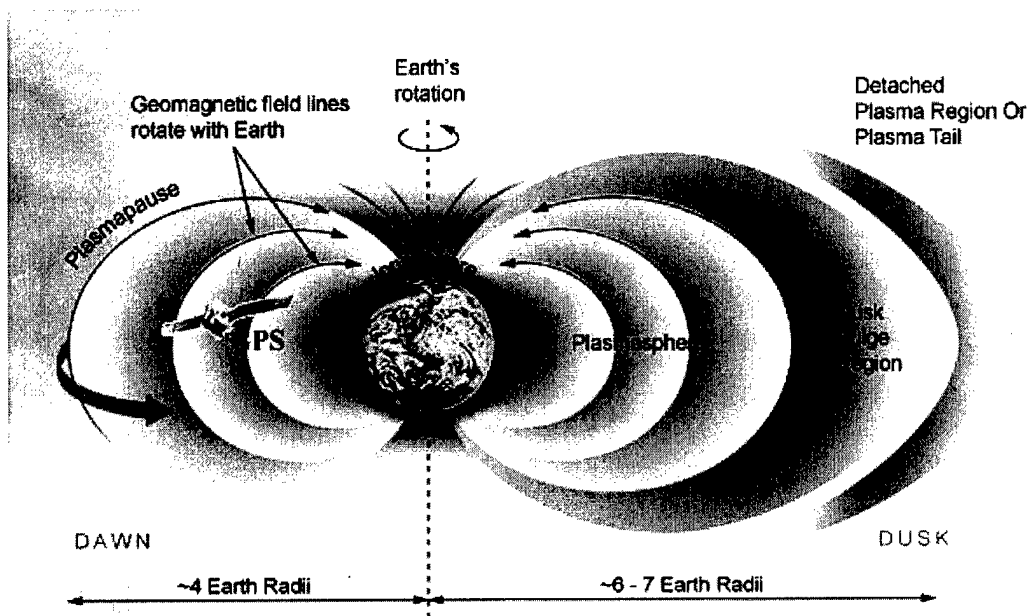
Figure 1: GPS and Plasmasphere Location [Johnson, 1999].

As mentioned above, almost all communication and navigational technologies in use today depend in some degree on the state of the ionosphere. Most satellites do not travel in orbits low enough to avoid the plasmasphere. For example, GPS (a non-stationary orbit)

2

travels at 20,330 km, and the geostationary GOES satellites reside at approximately 35,750 km. Both orbits are well beyond the topside of the ionosphere, and include the protonosphere. Specification by PRISM of the ionosphere alone is not sufficient to completely characterize the media affecting these devices. It becomes important to understand the contribution of this higher altitude plasma.

1.1.3. GPS Involvement

To help characterize the ionosphere, several measurement techniques are available: taking ionosonde measurements from the ground, sending up rockets and measuring directly the ionosphere in-situ, and even peering in from satellites passing high above. From those, GPS has been selected as the sole data source for two reasons. Both the availability of the measurements and the timely presence of the satellites within a global window provide an excellent data resource.

Ionosonde measurements have the advantage of looking vertically into the ionosphere, and measuring with great fidelity the electron density profiles up to a point. Once the peak electron density is reached (generally near an altitude of 290 km) the ionosonde signal is no longer returned, and no data can be gathered. Also, there are few ionosondes available worldwide, and they are fixed in location. Global coverage is severely limited.

Rockets traveling through the ionosphere taking in-situ measurements of electron densities are the most accurate and representative method. Of course, they are only infrequently used in experimental settings and cannot possibly provide the density of coverage needed. Also, not being space-based, they are limited to lower altitudes.

Certain satellites such as the Defense Meteorological Satellite Project (DMSP), have been launched with instruments capable of looking at ionospheric characteristics from

3

above at an altitude of approximately 840 km. In-situ measurements of H^+ density and ion drift velocities provide direct information about the plasmasphere. The problem is, again, there are few of these instruments active on board the current DMSP inventory, and the current coverage is neither global nor continuous. Measurements of electron densities would be sparse.

There is one source, however, that promises almost continuous global coverage: GPS Total Electron Content (TEC) measurements (described later in Section 0). With this global and continuous coverage, a quantified understanding of the sensitivity of PRISM to the GPS measurements would lend itself to gaining the advantages mentioned above.

Scope

This research compared the output values for PRISM run under three conditions: One condition used GPS TEC inputs which included the protonospheric contribution, the second was GPS TEC inputs with protonosphere excluded, and the third was with no TEC observation input (climatological mode). Comparisons were made among all three input conditions with the primary objective being to quantify the difference between PRISM run with protonosphere and PRISM run without. The values obtained this way are referred to as protonospherically distorted PRISM output.

Forty days, spanning the four seasons (January, April, June, and September) were analyzed. For each of the three conditions, the model evaluated data at fifteen-minute intervals for each day using the GPS TEC, Interplanetary Magnetic Field (IMF, B_z and B_y), Solar Sunspot Number (SSN), 10.7 cm flux (F10.7), and K_p inputs. The total executions with the 40 days of data came to 11,520 ([40 days] X [24 hours/day] X [4 15-minute

4

periods/24 hours] X [3 conditions]). With some additional post-processing of the output

files, the model data was then compared directly with the GPS TEC values.

2. Background

To understand the total picture, it's important first to understand the ionosphere and protonosphere, the total electron content (TEC) as it applies to these regions, the methods used in the measurement, and some of the science included in the PRISM model.

The Ionosphere
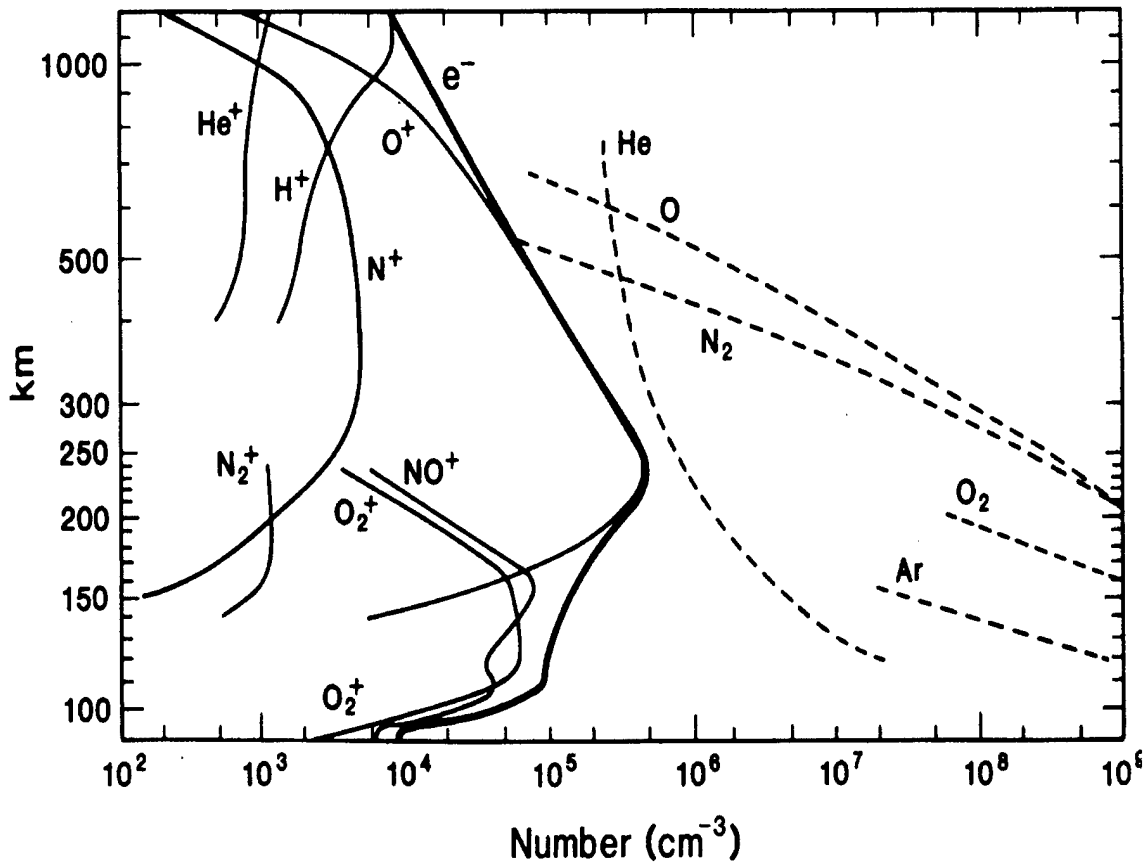
Figure 2: Daytime Ionospheric Profile [Johnson, 1969].

The ionosphere is a region of atmosphere with a high concentration of free electrons and positively-charged ions. Densities, measured in units of number per cm^3, range from less than 10^4 below 90 km altitude, to peak values of 10^6 at about 270 km. A complete treatment of the chemistry and physics of the ionosphere is well beyond the scope of this

text, what is presented here is a terse description of key features important to this study. For further information on the chemistry and physics of the upper atmosphere, see Rees [1989].

An experimentally derived picture of the earth's dayside ionosphere, shown in Figure 2, was derived from in situ measurements and remote-sensing data [Johnson, 1969]. Concentrations of common ionized and neutral species are charted by altitude as a function of density. Though the ionized species are important, it can be seen from the plot that neutral densities are still several orders of magnitude greater, particularly in the lower altitudes. Because of these density variations, the physics change as a function of altitude. The early investigators divided ionosphere into three majors regions: the D region (below 90 km), E region (between 90 and 130 km), and the F region (above 130 km). The F region is further divided into F_1 and F_2 since an additional feature sometimes appears below the main peak (F_2) [Kivelson and Russell, 1995]. The heights corresponding to the peak densities in regions E, F_1, and F_2 are designated h_mE, h_mF_1, and h_mF_2 respectively, with the corresponding resonant frequencies in these regions designated f_oE, f_oF_1, and f_oF_2.

There's no fine dividing line between where one process or constituent dominates the formation of any layer. The D layer is the lowest altitude and least dense ionospheric layer. Though not totally understood, it must be driven by only the most energetic solar and cosmic radiations since the upper ionospheric regions will absorb most of the energy before it gets to the D layer. The E layer shown in Figure 2, has a higher concentration of O_2^+ and NO^+ produced by ultraviolet radiation in the 100-150 nm wavelength range and solar x-rays in the 1-10 nm range. For F_1, the major constituent is O^+, and its peak occurs at about

7

170 km which coincides with maximum ion production by photons in the range from 17 to 91 nm [Kivelson and Russell, 1995].

For the F_2 region the controlling processes are much more complicated. Though production of O^+ is still the most significant source, species density is becoming such that several processes compete as the major loss mechanisms. O^+ recombination with electrons is one loss mechanism, however other processes such as disassociative recombination, diffusion, and drift are considerable losses that greatly complicate the region. It becomes impossible to calculate the height of density maximum in this region using the simple optical arguments applied previously, when the constituents are also subject to these additional losses [Kivelson and Russell, 1995].

Protonosphere (Plasmasphere)

Above the ionosphere is the region where a dominant concentration of ionized hydrogen (or protons) exists. The concentrations in this region are nominally 10^3 to 10^4 cm^{-3}. The ionosphere extends from approximately 90 to 1000 km. Here, singly-ionized atoms and molecules dominate. However, above that gravity causes a transition from relatively heavy atoms and molecules to the lighter protons (H^+). This is the region designated the protonosphere. Though no clear dividing line exists, once altitudes above 1000 km are reached it's easy to see the overall dominance of protons and singly-ionized He.

TEC

2.1.1. Normal TEC

Total electron content is a measure of the total number of electrons contained within a rectangular column of 1 m square. The calculation of TEC is accomplished by integrating the electron density along a given line of sight (LOS). TEC measurements are expressed in

TEC Units (TECu) or $10^{16}m^{-2}$. Typical mid-latitude values of TEC are in the range of 7 to

45 TECu, with the highest content occurring during midday. Higher values can occur

about the lower midlatitude and equatorial regions ranging from 70 to 80 TECu. The

horizontal map in Figure 3 demonstrates both of these features where the late evening

period is to the right of the map . Off the U.S. East Coast and into Eastern Canada, TEC's

have fallen to approximately 8 TECu, where southward off the West Coast of Mexico,

TEC's are reaching 70 TECu.
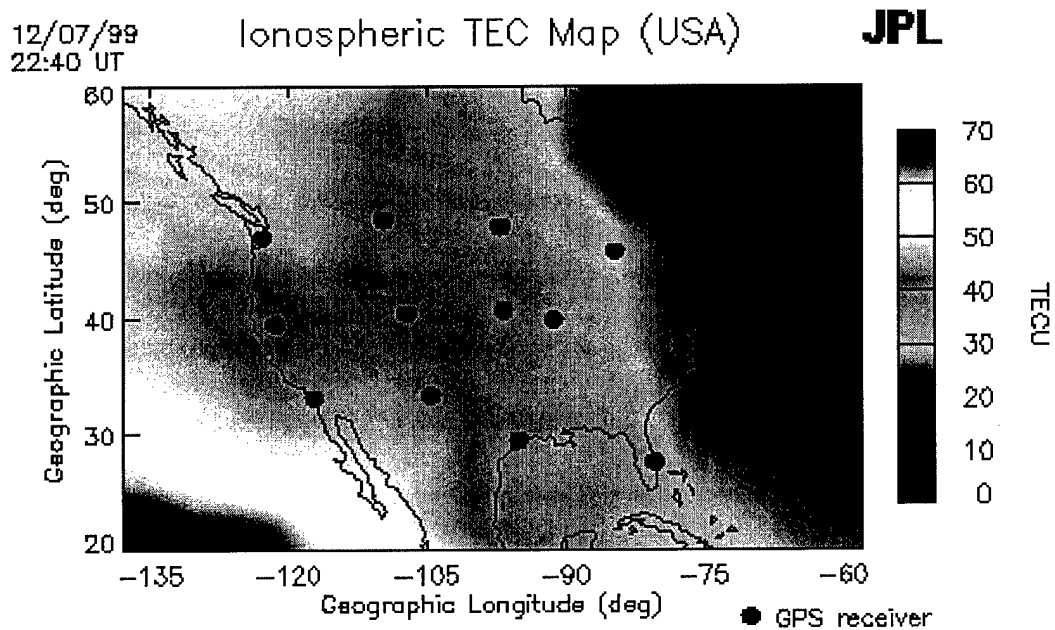
Figure 3: TEC Horizontal Map [Ziaoqing, 1999].

2.1.2. TEC in Protonosphere

In Figure 1: GPS and Plasmasphere Location, as the GPS travels from pole to pole, it

passes in and out of the plasmasphere. TEC measurements collected can include this

protonospheric content. Therefore, additional electrons elevate the TEC values measured

while the GPS is in the plasmasphere. Though the amount of distortion varies, a nominal

value for TEC in plasmasphere is 2 TECu near solar minimum at mid latitudes [Lunt et al., 1999]. During solar quiet periods, the plasmasphere region doesn't undergo diurnal variations as does the ionosphere, and without significant magnetic and solar activity, the densities above 1,000 km remain constant. So, when the TEC of the ionosphere fluctuates in a day from 7 to 45 TECu, the relative fractional fractional contribution of the protonosphere varies from 2/7 to 2/45. This can be even more significant during the winter months when TEC's can dip to 4 TECu at night, making the contribution as high as 50% [Lunt et al., 1999].

GPS TEC Measurements

The GPS network consists of at least 24 non-stationary satellites orbiting the planet at approximately 20,330 km altitude [AIAA, 1996]. On the ground, a continually growing network of dual-frequency receivers is used to measure TEC from the satellites. There are four important aspects to GPS TEC measurements; content of the measurement, how GPS TEC measurements are taken, how the data is accessed, and calibration.

2.1.3. What the Measurement Incorporates

Satellite signals can be passing through not only the ionosphere, but the plasmasphere (protonosphere) as well. Figure 1: GPS and Plasmasphere Location, shows the relationship between the GPS location, the ionosphere, and the plasmasphere.

Depending on the elevation angle of observation from the surface, and the position of the satellite at the time of observation, differing depths of plasmasphere will be present in the measurement. Typical values for this are discussed in Section 0.

2.1.4. How GPS TEC Measurements are Taken

The integrated electron density, TEC, is derived from radio signal response to electron content along the ray-path from the satellite to the receiver. The group velocity, v_g, of an electromagnetic wave is reduced, when compared to that of a wave traveling in a vacuum, by the presence of electrons (plasma). The group velocity in an unmagnetized plasma is the product of the speed of light in a vacuum and the index of refraction, $v_g = cn$. Since plasma has an index of refraction less than unity, the signals transmitted by the satellite travel slower than in a vacuum, and are delayed in their arrival at the receiver.

The GPS encodes its transmission with the time of transmission, or satellite time t_{sat}, when it sends a signal. This signal is received, after traveling through the atmosphere, at t_{rec}. This time of reception is compared to the satellite time encoded in the received signal, to establish a transit time, $\tau = t_{rec} - t_{sat}$. The satellite and transit times are then used as described below to establish actual range, pseudorange, and range-error.

11
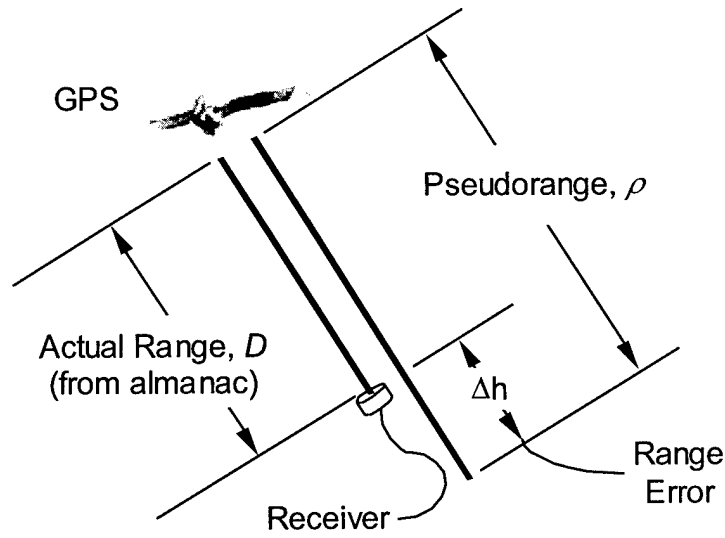
Figure 4: GPS Pseudorange Measurement.

Refer to Figure 4. To determine actual range to the satellite, the GPS position at satellite time is first extracted from almanacs of orbital information maintained by the U.S. Air Force (see Appendix C: Data File Manipulations). Then this position is compared to the receiver's position to determine actual range, D. Pseudorange, ρ, is the distance the signal would travel in time, τ, if there were no intervening material in the signal path. This value is the speed of light times the transit time, $\rho = c\tau$. Finally, range-error is defined as the pseudorange at a given frequency minus the actual range, $\Delta h = \rho - D$.

Derivation of the mathematical relationship relating pseudorange to TEC, begins with the basic form for the index of refraction. For a plasma, the index of refraction depends on both the plasma density and the frequency of the wave passing through it [Kivelson and Russell, 1995].

$$n = \sqrt{1 - (n_e e^2 / m_e \varepsilon_o)/(2\pi f)^2} \tag{1}$$

Here, n_e is the electron density, e the fundamental charge on an electron, m_e the mass of an electron, ε_o the permittivity of free space, and f the frequency of the transmission. With $m_e = 9.109*10^{-31}$ kg, $e = 1.6022*10^{-19}$ Coulombs, $\varepsilon_o = 8.854*10^{-12}$ Farads m^{-1}, and stating n_e in m^{-3}, f in Hertz, the equation reduces to

$$n = \sqrt{1 - 80.72\frac{n_e}{f^2}} \tag{2}$$

The quantity needed to obtain TEC, is the inverse of index of refraction, and can be approximated from the above equation by expanding the radical as shown below,

$$\frac{1}{n} \approx 1 + \frac{1}{2}80.72\frac{n_e}{f^2} = 1 + a\frac{n_e}{f^2} \tag{3}$$

where a = 40.35 m^3 s^{-2}.

To obtain range-error, begin with the range relationships. The actual range to a satellite, D, also defined as the Line Of Sight (LOS) distance, is extracted using τ and the almanac as mentioned previously. Pseudorange is further defined in terms of the group velocity, v_g.

$$\rho \equiv c \cdot \tau = c \int \frac{ds}{v_g} = c \int \frac{ds}{c \cdot n} = \int \frac{ds}{n} \equiv D + \Delta h \tag{4}$$

Substituting for the index of refraction as given by Equation 3, pseudorange for any frequency is given by the following approximation.

$$\rho = \int (1 + a\frac{n_e}{f^2})ds = \int ds + \frac{a}{f^2}\int n_e \cdot ds \tag{5}$$

$$\rho = D + \frac{a}{f^2}TEC \tag{6}$$

13

where TEC is defined as the integral electron density along the LOS, and D the distance integral along the LOS. Range-error can now be stated from the definition of pseudorange in Equation 4.

$$\Delta h = \frac{a}{f^2} TEC = D - \rho = D - c \cdot \tau \qquad (7)$$

The TEC for a given frequency can be determined by first solving for Equation 4 using the almanac value of D and measured τ. With only one frequency, the solution requires very accurate almanac data for each calculation of range-error. However, with two frequencies, TEC can be determined more precisely, and without almanac data, by evaluating the difference of the range-error measurements at each frequency, $\delta(\Delta h)$. Since the actual range, D, will be the same for each frequency, this differencing subtracts out the dependence on almanac data. A receiver uses this method to determine the error induced by ionospheric delay as shown below [Wells et al., 1986].

$$\partial(\Delta h) = (D - \rho_1) - (D - \rho_2) = \rho_2 - \rho_1 = \partial(\rho) \qquad (8)$$

$$\partial(\rho) = a \cdot TEC \cdot \left(\frac{1}{f_2^2} - \frac{1}{f_1^2} \right) = (40.28) \cdot TEC \cdot \left(\frac{1}{f_2^2} - \frac{1}{f_1^2} \right) \qquad (9)$$

where ρ_1 and ρ_2 are pseudoranges for frequencies f_1 and f_2 respectively, $\delta(\Delta h)$ is the difference between range-error measurements, and $\delta(\rho)$ the difference between pseudoranges for each frequency f_1 and f_2. When frequency is expressed in Hertz, TEC in electrons per square meter, and $\delta(\rho)$ in meters, a is approximately 40.28 m^3 s^{-2} as shown. From measurement, both frequencies and pseudoranges are known, and Equation 9 can be rearranged to solve for TEC.

2.1.5. GPS Data Access

GPS data is available from the National Geodetic Survey (NGS) web site, and is provided in Receiver Independent Exchange Format Version 2 (RINEX-2) [Gurtner, 1997]. Specifics on the format are contained in Appendix B: Receiver Independent Exchange Format Version 2.0. The format allows for several different receiver manufacturers, locations, and software implementations to use a single data structure. GPS observation files , which included header record information and observables, were used for this study.

The data files stated above contain timing, range and phase data needed for determining GPS TEC, but do not include information on the exact satellite position. For this, specification of the satellite orbits had to be calculated from almanacs. This was done using files available from the Air Force web site at Holloman Air Force Base, gpstest.46tg.af.mil/WebPub/General/BBS.inf ("Yuma" link). These files are available for user-selectable days, and specify in great detail the orbital information for all GPS satellites.

2.1.6. SCORE: Self Calibration Of psuedo-Range Errors

Self Calibration Of pseudo-Range Errors (SCORE) has been shown to reduce error in

TEC to within 0.5% of the actual value [Lunt et al., 1999]. The SCORE algorithm, detailed

in Appendix A: GPS Bias Calibrations (SCORE), derives from a self-consistency

condition involving several steps and assumptions. It's based on the following premise.

Satellites

Coincident IPP

Ionosphere

Observations
p2   p1

Earth's Rotation
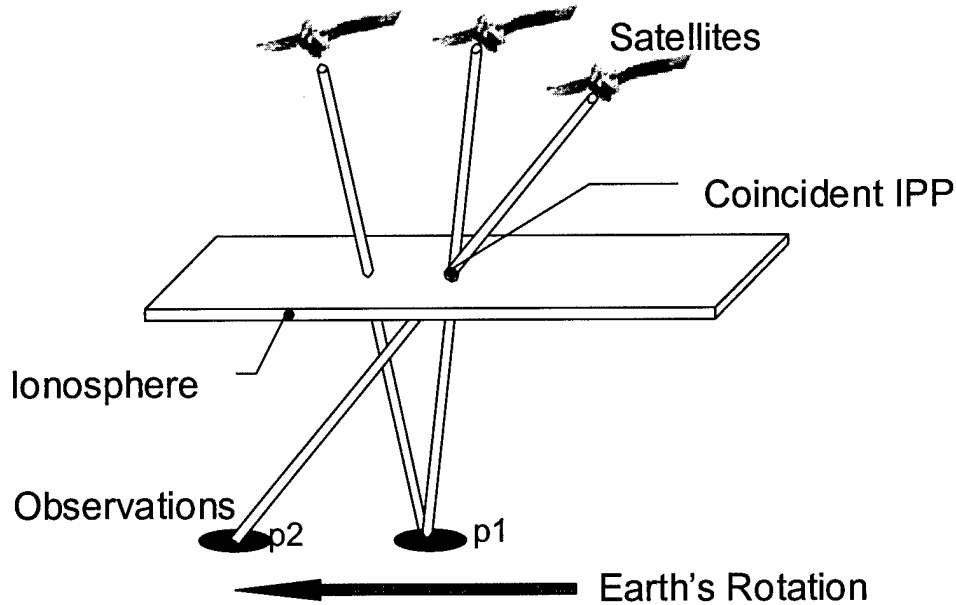
Figure 5: Satellite Ionospheric View Point Diagram.

If the LOS to two separate satellites are viewing the same point in the ionosphere, the

TEC they measure should be the same. In the Figure 5, three satellite's LOS are depicted.

The earth is rotating from right to left, the ionosphere is stationary with respect to the sun,

and the GPS travel as shown in the diagram. The SCORE premise is applied by specifying

each satellite pass as a function of the line it traces out in the ionosphere. The TEC

measurements associated with GPS LOS that pass through the same IPP are compared, and

the difference in the TEC measurement recorded as error. In this way, all GPS LOS for the

16

entire 24 hour period are collected and compared. The errors are minimized, leading to specific bias corrections for each GPS. This bias is then applied to each GPS TEC observation resulting in a self-consistent measurement of TEC for the entire period.

PRISM Science

Daniell and Brown [1991] developed PRISM, providing detailed documentation in their report. The code incorporates four physics-based models as a climatological core known collectively as the Parameterized Ionospheric Model (PIM). PRISM combines physical model outputs into a single global specification, then modifies that basis using both space and ground based data in a Real-Time Adjustment (RTA) algorithm to arrive at one or more user-selected outputs. Figure 6 demonstrates the basic data flow in PRISM.
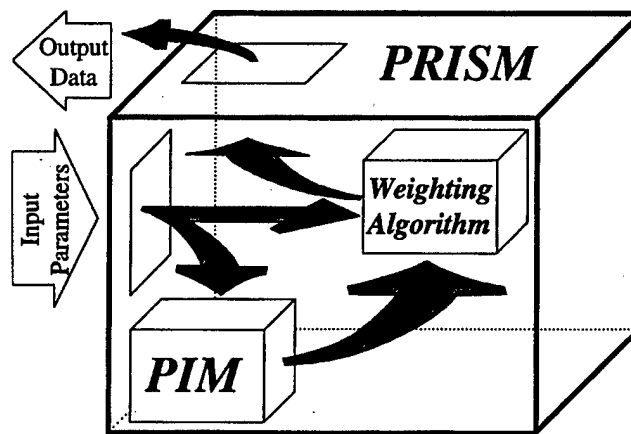
Figure 6: Data flow used in the PRISM process.

2.1.7. Physical Models (PIM)

PIM includes four models; the Low Latitude Model (LOWLAT), Mid Latitude Model (MIDLAT), Low- and Mid-Latitude E Layer Model (ECSD), and the High-Latitude Model.

LOWLAT was developed by Dr. David N. Anderson [1973] of the USAF Phillips Lab/Ionospheric Effects Branch, Hanscom AFB, MA. LOWLAT uses the empirical Ion/Electron Temperature Model developed by Brace and Theis [1981], neutral thermospheric winds from the Horizontal Wind Model (HWM90) [Hedin et al., 1988], and empirical models [Fejer, 1981; Fejer et al., 1989; Fejer et al., 1995] for empirical plasma drift velocities. MIDLAT is essentially the LOWLAT model, but with the equatorial dynamo electric field effects eliminated [Daniell and Brown, 1995]. The low and mid-latitude E layer model, E layer Continuous Slowing Down Model (ECSD), was developed by Dwight T. Decker and John R. Jasperse [Jasperse, 1982].

The fourth model is the Time Dependent Ionospheric Model (TDIM) developed by R. W. Schunk and J. J. Sojka at Utah State University (see [Shunk, 1988] for a review). An empirical high-latitude convection electric field [Heppner and Maynard, 1987] is used as well as the B3C electron transport code [Strickland et al., 1976; Strickland et al., 1994] and electron spectra from the Hardy et al. [1987] electron precipitation model.

2.1.8. Parameterization of the Physical Models

The physical models are continuous descriptions of global values. Due to limitations in computational resources, the continuum is parameterized in PRISM. This was done in two steps. First, only a specific number of geophysical and spatial conditions were used. Data is placed in bins with certain seasonal value, latitude region, solar activity, magnetic activity, and Interplanetary Magnetic Flux (IMF) direction. Second, since the basis model outputs were on different spatial grids, these outputs were approximated by a combination of tabulated values and Empirical Orthonormal Functions (EOFs) [Lorenz, 1956; Kutzbach, 1967; Davis, 1976; and Peixota and Oort, 1991].

2.1.9. Real Time Adjustment (RTA) Algorithm

The important features of the RTA are the available data and the regionalization of the adjustments. The near real-time data available comes from the Digital Ionospheric Sounding System (DISS), the Ionospheric Measuring System (IMS), and a suite of special sensors on the DMSP satellites. Important for this study is the IMS which is a network of dual frequency GPS receivers capable of measuring TEC. The RTA is split up into two regions: low to mid-latitude and high latitude. This division allows for a different adjustment technique in the complex upper ionosphere.

For low- and mid-latitudes, the output of the basis model is scaled using the observed values for six parameters: frequency of the F_2 layer density maximum (f_oF_2), frequency of the E-layer (f_oE), h_mF_2, h_mE, topside O^+ density, and the topside O^+ scale height. Though TEC data does not directly provide any of these values, PRISM does use it to modify the maximum ionospheric density (n_mF_2). This modified density is carried through the remainder of the RTA as a "driver" used to fit the basis model outputs. These fits are then globally corrected using a weighted average method.

For high-latitudes, instead of using an averaging method, the complexity dictates a further division into three regions. These are defined by the boundaries of the equatorward edge of the trough, the equatorward edge of the auroral oval, and the poleward edge of the auroral oval. Once these boundaries are established from observation, PRISM proceeds using a decision matrix based on the type and availability of data. For both the E and F layers, if there is insufficient data, a simple least squares adjustment is used to match intermediate values to the boundaries. For the F layer, better data lead to the use of a semi-

empirical f_oF_2 model (FMODEL) to adjust the TDIM O^+ profiles. The E layer uses a fast, first principles, local chemistry model (HLE) [Daniell and Brown, 1995].

Previous Validations of PRISM

2.1.10. Validation of Version 1.2

Validation was conducted by CPI [Daniell and Brown, 1994], comparing the results of PRISM to the then current Ionospheric Conductivity and Electron Density (ICED) model. The investigators used a data set including analog ionosondes, digisondes, polarimeters, incoherent scatter radars, DMSP instruments, and particle precipitation data from 9 October 1989. They divided the data into two sets; one set was used by PRISM to specify the ionosphere, and the other was taken as the ground-truth. Comparisons were made for the output of PRISM and the ground-truth data with PRISM producing on average a 56% improvement in accuracy over ICED. Other data were compared. But, for this present study, the most relevant error was the measure of TEC. PRISM was found to have a TEC RMS error of 8% [Daniell and Brown, 1995].

2.1.11. Validation of Version 1.6b

David Coxwell [1996] performed a validation of PRISM using DISS and GPS TEC from the solar quiet data months March 1994 through January 1996. PRISM calculated TEC at 0000L, 0600L, 1200L, and 1800L at two latitudes (30° N and the equator) for three seasons (Equinox, Summer, and Winter). These data were then compared to ground-truth values taken from NASA's dual-frequency radar altimeter on the TOPographic EXperiment (TOPEX) satellite during 1995. This satellite is a low-earth orbiting satellite primarily designed to measure sea-surface heights. It's data represent ionosphere-only TEC values, but only over the oceanic surfaces.

He determined the radius of influence of a single real-time observation was

approximately 2,000 km from the observation station. Outside this radius, model outputs

with real-time inputs were identical to those without. Combining all the possible

observation sites, this leaves over 76% of the earth's surface outside the influence of

PRISM's RTA. Another conclusion was PRISM TEC calculations driven by DISS data

generally performed worse than PIM alone during equinox seasons; however, they had a

slight advantage during summer and winter solstices. Finally, when driven by GPS/TEC

data, the model did well against PIM in the mid-latitude regions in the summer, fall, and

winter; but not for equatorial stations. It was not clear if this was a protonospheric effect.

2.1.12. Validation of Version 1.7b

Shawn Filby [1997] executed PRISM using GPS TEC and DISS data at two different

stations, Wallops Island, Virginia, and Point Arguello, California. The model was run

three times for each station with the first run being without real-time input (PIM only). The

second run used GPS TEC data only as the input, and the third was done with GPS TEC

reduced by 4 TECu in an attempt to correct for the plasmaspheric distortion. The DISS,

which does not include the plasmasphere, was used directly as ground-truth for each of the

model runs.

He found, among other things, that the model over-predicted TEC when using GPS TEC

data. Accordingly, PIM was able to better specify TEC related values. He also found an

under-prediction in h_mf_2 during the nighttime hours. It was unclear if the bias was due to

the model used in PIM for the high altitude horizontal winds or a deficiency in the RTA. A

couple of surprises came from the model reaction to the periods at sunrise and sunset. Here

there was an unexpected increase in only the h_mf_2 values when PRISM ingested GPS TEC

21

values. This shouldn't occur since the RTA scales the entire layer due to inputs, and shouldn't affect any given peak altitude. Along these lines, there was also a pre-sunset enhancement of h_mf_2 at the lower latitude station. This was an amplification of the previous error. Using the GPS TEC values reduced by four did not improve the response for any measurement except at the lower latitudes during the summer equinox peaks.

2.1.13. An Application of PRISM to Regional Ionospheric Specification

The group from the Air Force Research Laboratory, Space Vehicles directorate (AFRL/VSB) [Bishop et al., 1999] has initiated an analysis using PRISM 1.7c. Though the architecture of the study is not intended as a validation, it does represent an opportunity to compare PRISM's outputs to real data.

They used ionosonde and GPS data only to compare the outputs of PRISM within a small regional window directly above the Croughton IMS in the United Kingdom. The model was driven four ways; one with no inputs, another with ionosonde only, GPS TEC only, and finally with both. With the GPS observed TEC values taken as ground-truth, the model's outputs were plotted in several ways showing differences between this ground-truth and PRISM output.

The study was intended as an initial architecture of regional specification using the PRISM model. Neither enough types of data, time periods, nor spatial separation were employed to arrive at any statistically significant figures. There were some interesting results, however. The median ratio of PRISM's TEC output which had plasmaspheric contribution, to observed TEC was 0.946. The corresponding difference between PRISM TEC and observed was –0.85. For this individual data run PRISM appears to be under-predicting TEC.

The study does present comparable figures for the data and output streams and should

be continued over longer periods and various regions. Contributions from error sources

such as the plasmasphere need to be addressed, and better data assimilation methods need

to be employed.

3. Research Method

There were several procedural decisions made ranging from selecting the best site and data set, to how the comparison and statistics should be compiled. What follows here are specific details on these decisions, and a general summary of the actual methods used.

Raw Data and Site Selection

3.1.1. Data Types

The data types fell into two categories; GPS TEC, and PRISM auxiliary. Consistent with the reasons stated in Section 1.1.3, GPS TEC was selected as the primary data type. With the scope of this study considering only the plasmaspheric affects on PRISM, it was important to restrict data to those that could be divided into groups. GPS can be segregated into one group relatively free of plasmaspheric content, and another with a definite contribution. Though PRISM accepts inputs from various data sources, none of the other sources could be so well categorized. DMSP satellite data is too sparse, and the measurements it takes are too low in altitude to include plasmasphere, DISS likewise does not include protonosphere in its measurement, and in situ rocketry data is not an active source.

All the data needed for auxiliary input to PRISM was available and used. Details on content and availability can be found in Section 3.1.7, with file format and access procedures in Appendix C: Data File Manipulations.

3.1.2. Site Selection

There were two drivers for site selection: For one, a calibration latitude cutoff, used to separate GPS TEC measurements into those containing plasmasphere, and those that do not, had already been established for Pittsburgh. GPS bias calibration can be improved to

24

within 0.5 TECu of actual values at all times and for all seasons [Lunt et al., 1999]. This is done by selecting a minimum acceptable latitude, below which TEC measurements would not be used in the bias calculation. For Pittsburgh, PA, the latitude at which plasmaspheric distortion had the least effect on GPS bias calculations has been established [Law, 1999]. Figure 7 contains an example of the impact of latitude cutoff. At the poleward latitudes (32° N to 40° N), very little data is available for calibration, and the TEC measured is noisy and elevated due to the sparse data. As the LOS moves down in latitude (> 40° N), it begins to include protonosphere and the average TEC measured is elevated. The minimum average TEC measure on Figure 7 represents the point where both the protonospheric enhancement and the effect of poleward data reduction are minimized. This value was 40.75° N for Pittsburgh, and became the low-latitude cutoff.
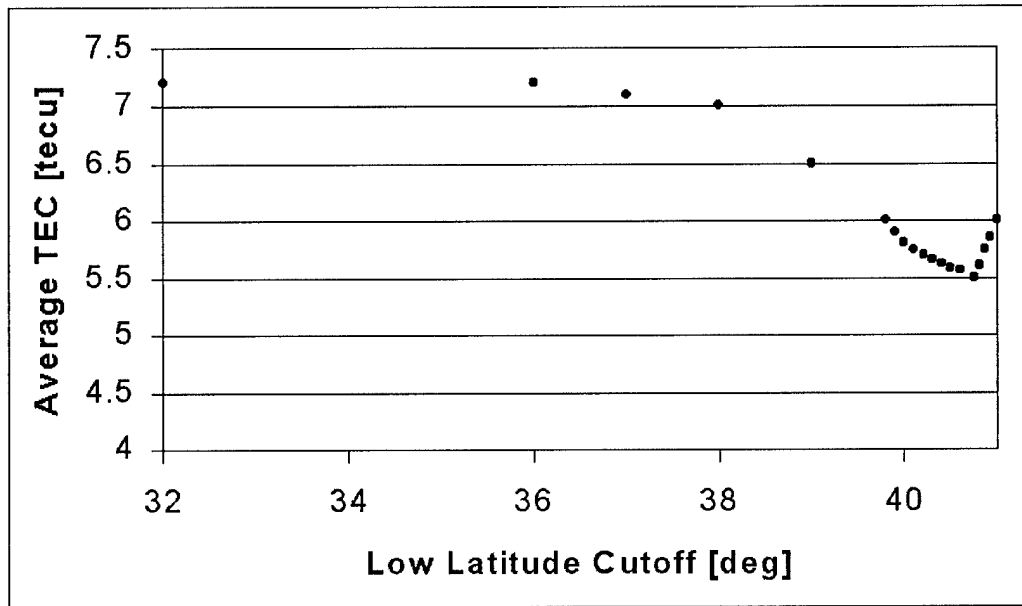
Figure 7: Low latitude cutoff impact on GPS TEC [Law, 1999].

Secondly, Pittsburgh's location lent itself well to peering into both plasmasphere and undistorted ionosphere from a single point on the surface. With the latitude cutoff taken as

the point where the plasmasphere has the least effect, we still have a great deal of room to view the ionosphere above the cutoff. Figure 8 demonstrates the relative split in regions with and without plasmaspheric content. With the observational window ranging from 4.52° to 76.59° (see Section 0 Grid Manipulations), 40.75° divides the regions almost perfectly in half. This study quantifies this contribution, and Pittsburgh's position provides a good split in this data availability.
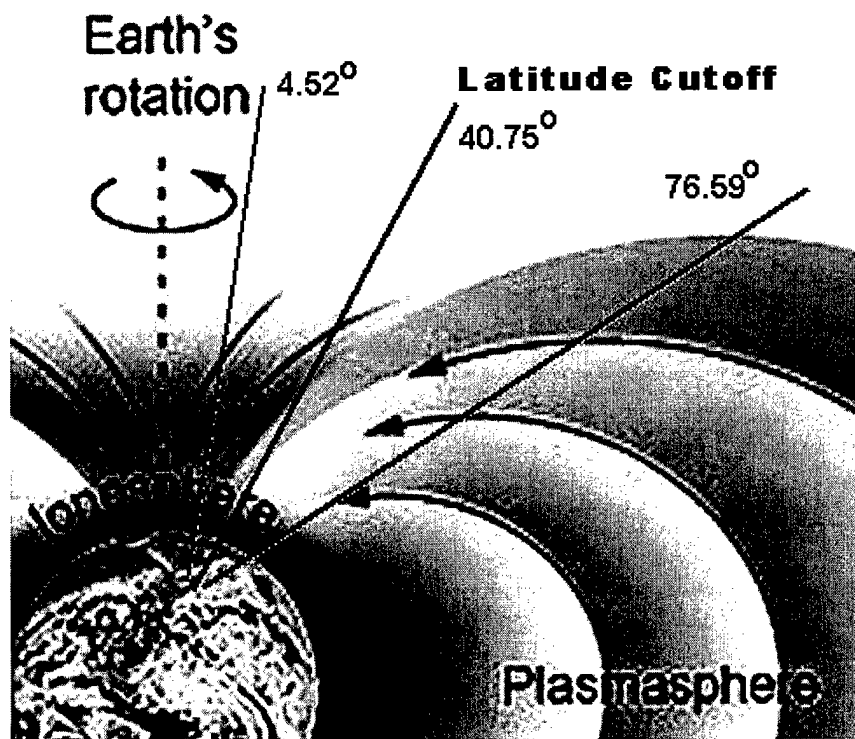
Figure 8: Latitude cutoff regions.

GPS TEC Data Manipulations

Methods for the handling of GPS TEC data are shown below with specific details covered in Appendix C: Data File Manipulations, and analysis in Section 0.

3.1.3. Pittsburgh Anti-Spoofing

An important first hurdle to cross was a missing column of data in the Pittsburgh GPS files. This missing column was due to Anti-Spoofing (AS); a method used to reduce the possibility that a GPS signal could be mimicked. The normal transmission codes carried in the two GPS frequencies are modified to literally complicate reception. Normally, among other data, Coarse Acquisition (C/A) is carried on frequency L1 and Precise (P) codes are carried on both L1 and L2. TEC calculation would like to use the range information from the P codes since they are the least noisy. But, under AS conditions, the P code from the L2 frequency (P2) is re-coded and carried in L1 in the new form. To rebuild the P2 signal requires the receiver to break down the modified code carried in L1 into its original P2 form. The receiver at Pittsburgh doesn't do this. Therefore, P2 data is simply not available.

Since the calibration requires two pseudorange measurements to calculate TEC using Equation 9, a substitution is made when reading the data files. Range information in the C/A code (C1) is noisier, but follows closely the range measure in the P code. So, data in the C1 column was shifted substituting C1 for P2. Increased noise is present, but the dual-frequency range data is now available.

3.1.4. GPS TEC Calibration

Calibration was actually managed in a number of steps; transformation of the RINEX-2 observation file to Differential Group Delay (DGD) and Carrier Phase (CP), checking for wild data points, fixing data discontinuities (or jumps), visually editing and reviewing these fixed files, then calculating bias using SCORE. Specific details on this process are contained in Appendix C: Data File Manipulations, and Appendix A: GPS Bias

27

Calibrations (SCORE). This procedure was followed for each raw data file with AS correction employed, a latitude cutoff of 40.75° N used, and a MathCad algorithm executed to further smooth data.

In order to assess the sensitivity of the data set to a specific calibration procedure, some files were also calibrated under slightly different conditions: Data from 1997, days 70-76 and 175-180 were calibrated with latitude cutoff and without. Figure 9 shows one of these days. On the main plate, the equivalent vertical TEC is plotted for each satellite pass as a function of Ionospheric Penetration Point (IPP) local time. IPP is taken as the point in the ionosphere where the LOS from GPS to the receiver intersects 350 km altitude. IPP local time corresponds to universal time (UT), and depends on the IPP longitude position with respect to the prime-meridian ("location" of zero UT). IPP local time is UT plus IPP longitude (where West is +, and East is -) divided by 15°. On the lower plate, the latitude position of the satellite pass is traced as a function of IPP local time. For example, look at a satellite pass, select the trace which begins at -4h. The latitude trace can be seen moving upward as time passes. There is a corresponding VTEC beginning at 8 TECu in the upper plate whose starting point is lined up exactly vertical of the latitude trace. The VTEC value initially decreases as a function of time, then begins to increase at about –2h, terminating at its maximum of 8 TECu.

On the figure, there are two VTEC plots overlaid. One is the IPP data with the SCORE (see section 2.1.5) bias applied that has not had the cutoff latitude implemented. The other has had the cutoff employed in calculating bias. The SCORE process only uses specific latitudes to calculate the bias. But, once the bias is determined, it's applied to the entire measurement data set. This is why values below the low-latitude cutoff still appear on the

plot for both implementations plotted here. Consistent with previous findings [Lunt et al.,

1998], the difference is approximately 2.5 TECu, and represents the contribution to GPS

TEC by the plasmasphere.
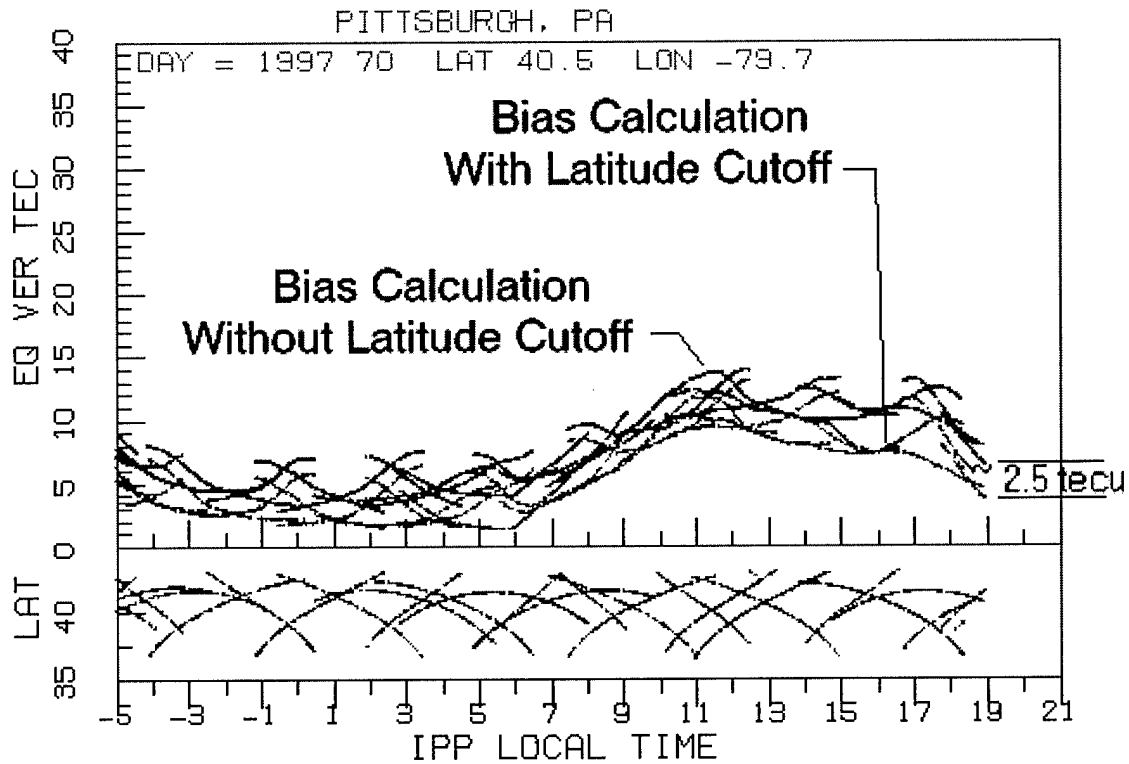
Figure 9: Bias Calculated With and Without Latitude Cutoff.

3.1.5. Slant TEC to Vertical TEC

Once the calibrations were complete, the data had to be transformed to a PRISM input

format. The calibrated data contains Observed Slant TEC (OSTEC) from Pittsburgh along

LOS to all GPS satellites. During the 1997 runs, these data were recorded every 5 seconds,

and during subsequent years, every 15 seconds. PRISM needs an input of Observed

Vertical TEC (OVTEC) specified in a horizontal grid with each of the values observed

within the same time bin.
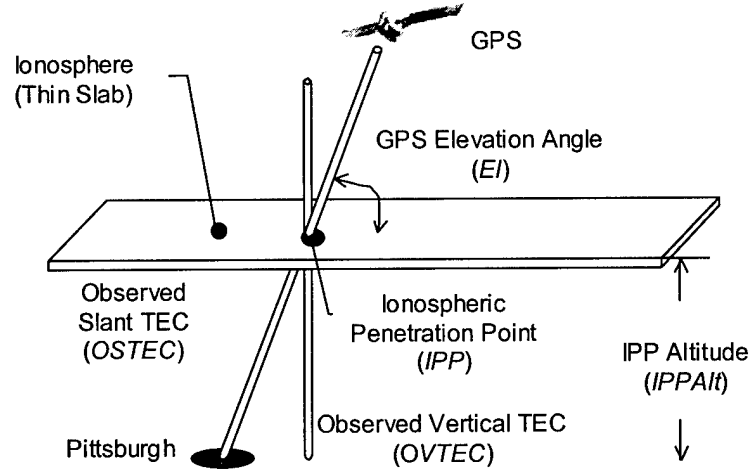
Figure 10: OSTEC and VTEC Diagram.

Figure 10 diagrams the geometric relationship between the two TEC measures. The LOS from Pittsburgh to the satellite represents an STEC measurement, with the corresponding VTEC column going through the same IPP. Elevation angle and IPP altitude will have direct affect on the conversion to VTEC.

To convert OSTEC to OVTEC, the ionosphere is approximated as a thin slab containing all the electrons, with constant density and a topside altitude of 350 km [AIAA, 1996]. This allows for a simple geometric model shown in the equation below [Andreasen et al., 1998].

$$OVTEC = OSTEC\left(\cos(\sin^{-1}(\frac{R_e}{R_e + IPPAlt} \cdot \cos(El))) \right) \qquad (10)$$

Here, OSTEC is the Observed STEC in TECu, R_e is the radius of the earth in km, IPPAlt is the IPP Altitude in km, and El is GPS elevation stated as the angle from the observer to the satellite. Though the equation allows for any value of IPP altitude, the standard is taken at 350 km.

To test the accuracy of the thin shell approach, a single PRISM output grid was selected from the data set that did not include any significant geomagnetic activity. First, PRISM STEC (PSTEC) was calculated by integration of the PRISM output grid along each LOS for a specific satellite pass that included elevation angles ranging from 13° to 80°. From this PSTEC data set, PVTEC was calculated in two ways: Method one simply used Equation 10. The second method used the same grid, but VTEC was determined by directly integrating the PSTEC data set vertically at each IPP.

The results for these two calculations for an IPP altitude of 350 km are shown in Figure 11. Since this satellite pass never went directly overhead, the graph never reaches an elevation of 90°. The rapid rise in VTEC below 20° appears because the LOS now includes a large portion of the protonosphere. The LOS looking equatorward at 20° elevation and below intercept the plasmasphere, while those looking poleward do not. The equatorward VTEC's are therefore elevated relative to the poleward values. For elevations greater than 20°, there's excellent agreement in VTEC values for all elevations up to 40°, where the apparent split just after 40° demonstrates again the protonospheric effect. The higher TEC values indicate the satellite is approaching from a position below the latitude cutoff. And even in elevations above the 40.75° N cutoff, a small contribution from plasmaspheric electrons is seen. Half of the low elevations were looking into plasmasphere, while the other half were looking poleward.

31
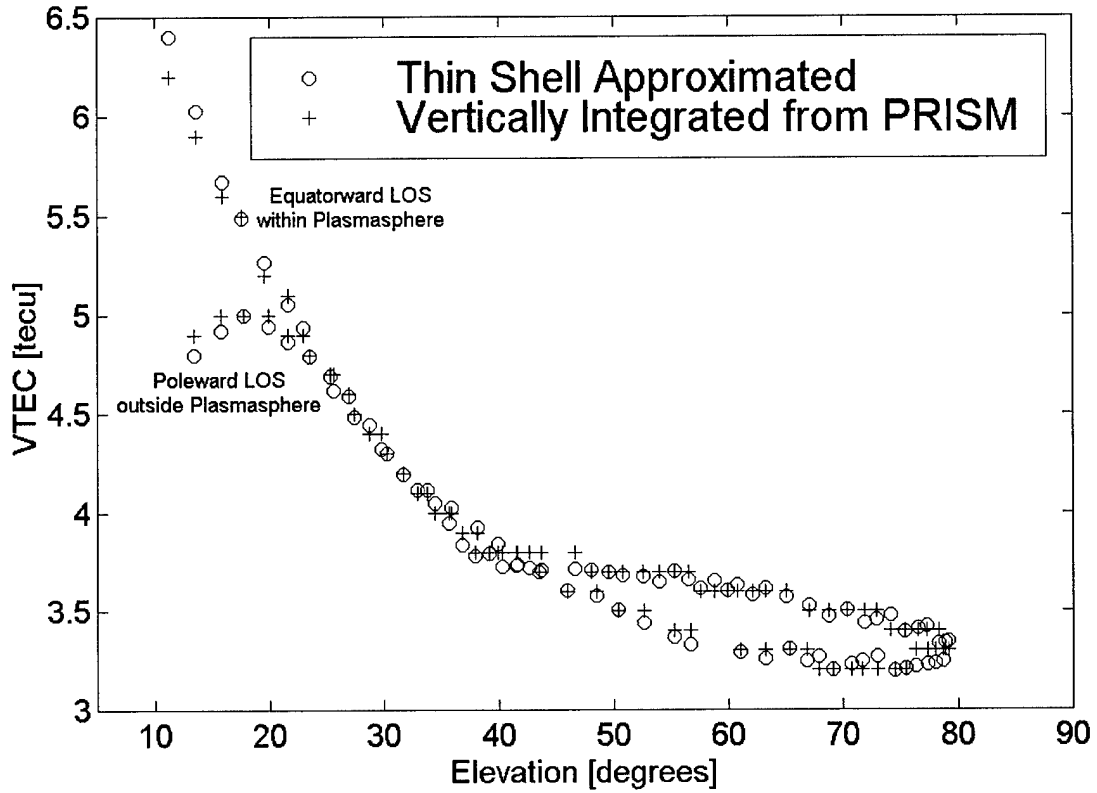
Figure 11: Thin Shell Approximation Comparison at 350 km.

The maximum difference between the approximation and the vertical integration as a function of IPP altitude is plotted in Figure 12. A minimum error of 0.143 TECu occurs at 340 km, with a 0.201 TECu difference at 350 km. With the nominal values of 45 TECu, this represents an error of 0.45% for VTEC approximated at an IPP altitude of 350 km. If the minimum in this case were used, there would only be an increase of approximately 0.13% accuracy over the nominal 350 km IPP value.
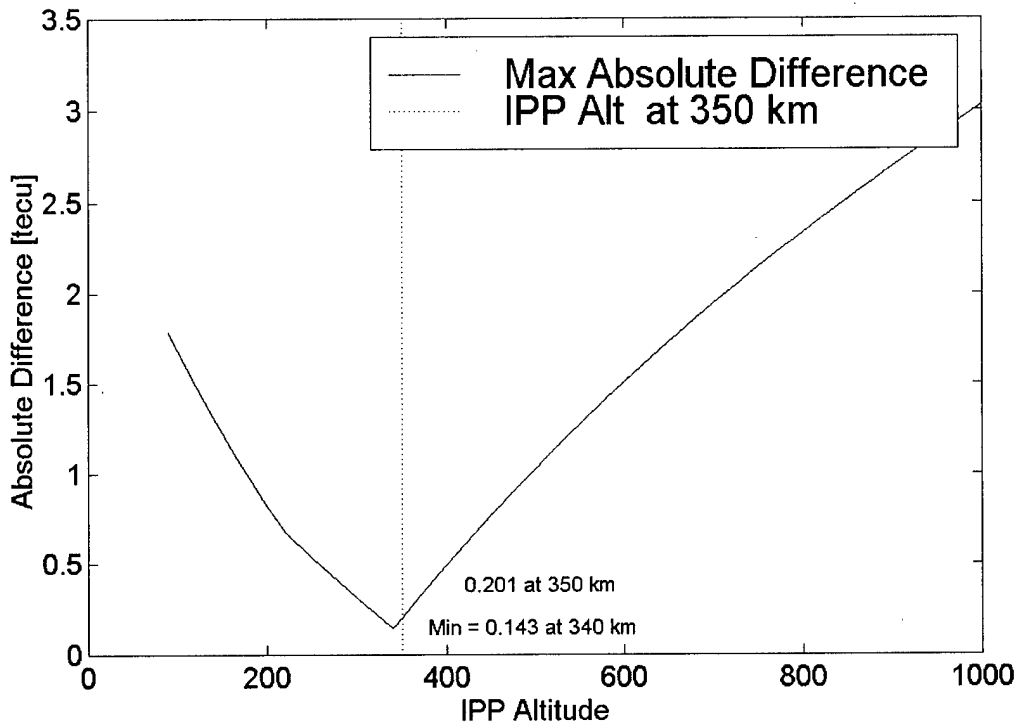
Figure 12: Thin Shell Approximation Absolute Differences.

Though this appears to be on the same order as previously reported accuracies of 0.5% [Lunt et al., 1999], this high degree of accuracy is quickly overwhelmed by the approximation of the horizontal gradient-free ionosphere used in the VTEC conversion. For example, in Figure 3 the gradient in VTEC is plotted across North America. When the 6° x 9° IPP window is overlaid on the map over Pittsburgh, a difference of approximately 10 TECu can be seen from the far Southwest to the Northeast. The gradient is significant, and becomes an important source of inaccuracy in the thin shell approach.

PRISM Model Runs

Once the data type, calibration method, and site had been selected, what remained was to execute PRISM following the procedures contained in Appendix C: Data File Manipulations.

33

3.1.6. Data Preparation

Three separate data folders were compiled; one containing all OVTEC values converted from the OSTEC, a second with only those OVTEC values above the 40.75° N latitude cutoff, and a third with no data.

3.1.7. Auxiliary PRISM Input Data and Availability

Other inputs needed for the PRISM model include f10.7, Kp, Sunspot Number (SSN), and interplanetary magnetic field values. The solar activity data (f10.7, Kp, SSN) are available in single files from the National Geodetic Data Center (NGDC) FTP site: ftp.ngdc.noaa.gov/STP/GEOMAGNETIC_DATA. Interplanetary Magnetic Field (IMF) data was available from two different satellite sources both on the NSSDC web site: nssdc.gsfc.nasa.gov/space. These web sites also provided descriptions on format and content for each of the data values. A short discussion on each data value follows.

The Ottawa 10.7cm solar radio flux is adjusted to 1 astronomical unit (1 AU) each day. The measurement is taken at 17:00 UT each day and expressed in 10^{-22} Watts meter^{-2} Hz^{-1}. The planetary 3-hour index K_p is the mean standardized K-index from 13 geomagnetic observatories between 44° and 60° N or S geomagnetic latitude. This index is designed to measure magnetosphere-ionosphere disturbances by quantifying their magnetic effects. K_p ranges from 0-9 in thirds of a unit with values above 3 representing active periods. The International Brussels number is provided here as the Sun Spot Number (SSN). This value is not a derived value, and is therefore independent of the f10.7 data. There are two main sources available for IMF data: The IMP-8 (IMP-J) and WIND satellites both measure magnetic fields (among other things) from an elliptical orbit of approximately 235 Earth Radii within the L1 region. Magnetic field data in the form of B_z and B_y are provided by

the two spacecraft. Two sources were selected since there are periods when one satellite did not have a value available. Fortunately, for all of the executions in this study there were IMF values from one or the other source.

Grid Manipulations

Two "grids" were employed in this study; the user-friendly 9-point horizontal grid used for comparing PRISM outputs, and the PRISM input grid.

3.1.8. Horizontal Grid

As discussed in Section 2.1.13, a user-friendly 9-point grid has been adopted [Bishop et al., 1999] to compare various horizontal values. Here, PSTEC is calculated, and averaged into evenly spaced horizontal bins defined by this grid. The 9-point grid is itself derived from the IPP window as shown in Figure 13. Here, a numbering convention for each of the bins was adopted to simplify visualization and discussion. These numbers are seen in the grid diagram below.
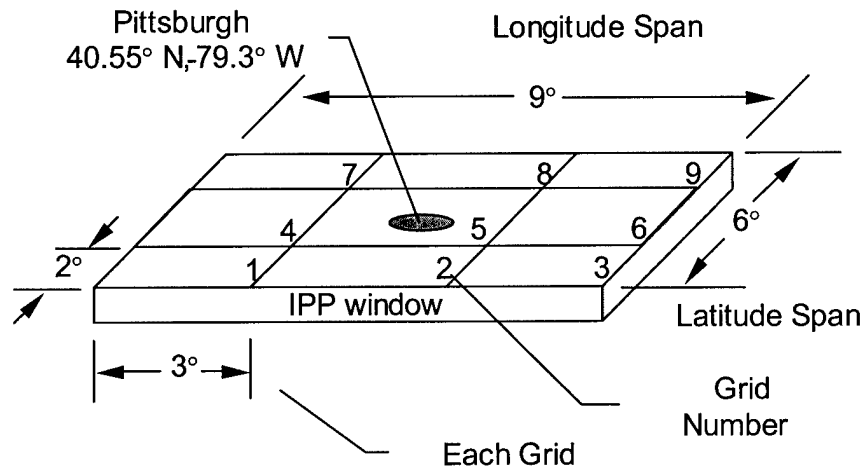
Figure 13: User-Friendly 9-Point Grid.

Several factors impacted the definition of the IPP window. The radius of influence [Coxwell, 1996] initially limited the span to 2,000 km at the furthest point. At IPP altitude (350 km), a degree of latitude equates to roughly 117 km. And at Pittsburgh's latitude, a degree of longitude is approximately 83 km. The total span becomes 703 by 746 km with a maximum distance of 1025 km (corner to corner).

PRISM weights the driver station influence as a function of horizontal distance as shown in Figure 14. For practical use, all the distances inside of approximately 12.5 km use a weighting factor of unity. The remaining weighting factors fall to zero by approximately 500 km. The decorrelation length of the ionosphere is of the order of 1000 km or less, and this weighting function falls well within that constraint [Daniell and Brown, 1995]. Though this disagrees with the 2,000 km value, it has no impact on the methods used in this study. The SCORE calibration is based on close proximity of individual measurement locations. Therefore, when the calibrated GPS data is input into PRISM, it is necessarily within the 600 km distance shown below.
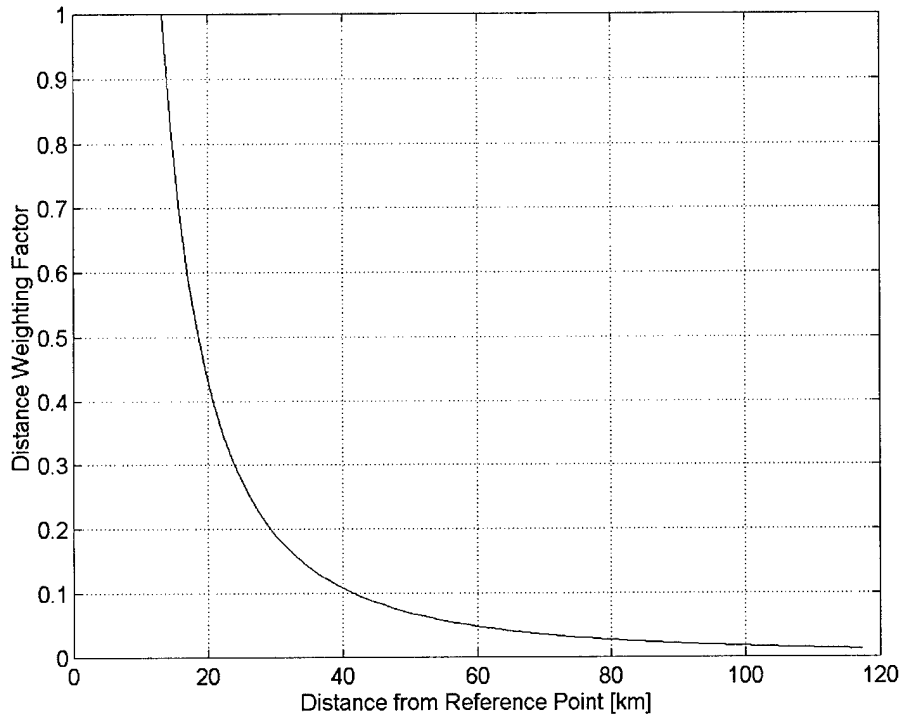
Figure 14: Horizontal Driver Station Influence as a Function of Distance.

The elevation angle for viewing the GPS satellites was also a strong consideration.
Looking too low on the horizon can cause extensive noise due primarily to the amount of
atmosphere being viewed and the multipath errors from surface objects. Though not
noise free, a 15° elevation angle [Bishop et al., 1999] has been found to partially suppress
the horizon noise. With the surface again estimated as flat, the maximum distance of
1025 km, and the IPP altitude of 350 km, the minimum elevation angle out to a point on
the corner of the IPP window is 18.5°. This again falls within the minimum allowable
target of 15° mentioned above.

Output of PRISM had to be integrated along slant paths to establish PSTEC values for
comparison to GPS measurements. To facilitate this, the grid used in PRISM had to

incorporate an IPP window larger than 6° latitude by 9° longitude to capture all the TEC along the LOS. Figure 15 demonstrates the latitude geometry for this window calculation. Here, when the GPS receiver is looking through the IPP window at an IPP latitude, the satellite orbital latitude is different. The highest value for orbital latitude is labeled in the figure as "PRISM Maximum Latitude," and there are corresponding intersections for the minimum latitude and longitude boundaries (not labeled). These limits become the IPP boundaries needed by PRISM to integrate TEC up to GPS altitudes.
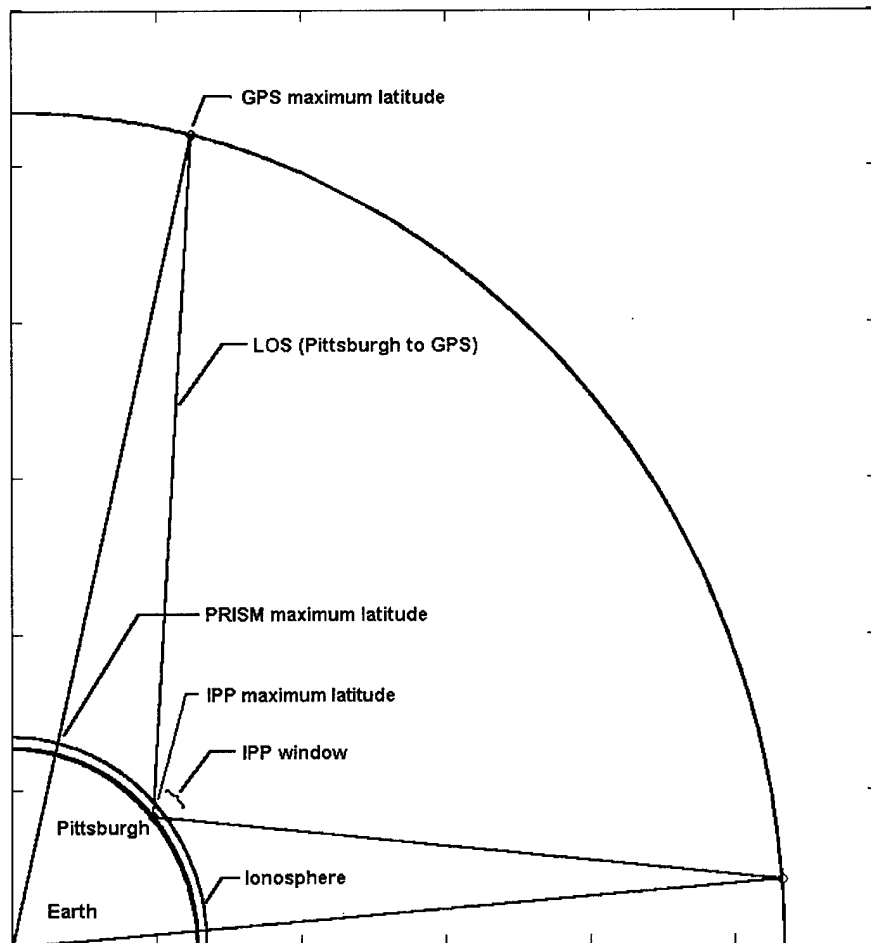
Figure 15: IPP Latitude Window, General.

Determining the bounds of the PRISM execution grid involved two steps. First, the position of the satellite at minimum and maximum IPP window points had to be determined. A line drawn from Pittsburgh through the IPP boundary was extended to GPS altitude, and that intersection became the latitude limits for the PRISM grid. Also, by approximating the surface of the Earth as flat, the Pittsburgh elevation angles for points on the IPP window were also determined. A similar calculation was done for the longitude portion of the IPP window. The grid needed for PRISM to fully encompass both the ionosphere and plasmasphere up to GPS altitudes was found to span approximately 72° latitude, 72° longitude, again centered at Pittsburgh's 40.55° latitude., -79.3° longitude.

3.1.9. Altitude Grid

The default altitude grid for PRISM, shown in Table 1, is 50 unevenly spaced points covering altitudes ranging from 90 to 1600 km. The uneven spacing comes from the normalization methods used to parameterize the basis functions used in the model. The range is set to cover the nominal height associated with significant O^+ densities [Daniell and Brown, 1995] as shown in Figure 2. PRISM does not include a protonospheric model, and in its current form, will not model the H^+ densities above 1600 km.

Table 1: PRISM Default Altitude Grid.

90.000	95.000	100.000	105.000	110.000
115.000	120.000	125.000	130.000	135.000
140.000	145.000	150.000	160.000	170.000
180.000	190.000	200.000	210.000	220.000
230.000	240.000	250.000	260.000	270.000
280.000	290.000	300.000	320.000	340.000
360.000	380.000	400.000	450.000	500.000
550.000	600.000	650.000	700.000	750.000
800.000	850.000	900.000	1000.000	1100.000
1200.000	1300.000	1400.000	1500.000	1600.000

In hopes of increasing the resolution, the grid was first adjusted to an evenly spaced 100-pt grid within the same limits. This led to model and post processor run times that are on the order of 45 seconds for a single data file, and output files on the order of 12 MB in size. With as many as 11,520 data files, this would have taken approximately 144 hours to run, and 138 GB to store! Though the run times were manageable, the storage requirement was unacceptable. Cutting this grid by half to the default 50 uneven points reduced the run time to 135 hours or by 6.3%, and the storage requirement to approximately 6 GB. It is not clear why a 50% reduction in data points calculated by PRISM only reduced run times by 6.3%. Nominal run times when using a horizontal grid of 15 by 15, and the default elevation 50-point grid, resulted in run times on the order of 4 seconds. This represents a 97% reduction in data points calculated, and a 96% reduction in run times. Again, the relationship between the number of points in the elevation grid and model run times is undetermined.

PRISM Post-Processing

After each of the data sets were run, the gridded electron density profiles were processed first by converting to PSTEC, then sorting the data into bins based on both horizontal grid location and elevation, with the final step being visualization and recording of the comparison.

3.1.10. Gridded Output to Slant TEC

There are two ways to compare observation files with PRISM output: one is to use the OVTEC calculated by the thin shell approximation with PRISM's VTEC (PVTEC), the other is to convert the PRISM's gridded output to STEC (PSTEC), and compare with

OSTEC. The horizontal gradient error discussed in Section 3.1.5 is considerable, and more importantly not well defined. This error directly affects the conversion of OSTEC to VTEC via Equation 10, but does not directly affect integration used to calculate PSTEC. Since the calibrated OSTEC was the real measure without approximations, it made more sense to integrate PRISM for the comparison.

The output of PRISM forms a three-dimensional grid with electron densities specified at geographic latitude, longitude, and altitude throughout the user specified window. To convert this to PSTEC, the densities are simply integrated along a series of LOS's using each of three numerical integration methods; Romberg, spline, and trapezoid. All comparisons in this study use the spline integration method to allow for inclusion of the endpoints in the data set. The other two methods were unused.

3.1.11. Production of Distribution Bins

The output data was separated into both horizontal grid and elevation angle bins in accordance with specific details in Appendix C: Data File Manipulations. In summary, data was extracted from the PSTEC outputs and stored in separate files, then these files were individually manipulated using Matlab algorithms to perform plotting and comparison statistics.

There were two sets of data bins produced; the 9-point horizontal grid discussed in Section 0, and elevation angles. Elevation angles were divided from 16° to 90° by increments of 2° resulting in 37 evenly spaced bins. For each of the bins, PSTEC was extracted and written to individual files. With the 9 horizontal grids and 37 elevations, this totaled 46 bin files for each data day's output. These were then passed on to the Matlab visualization and statistical algorithms.

3.1.12. Visualization and Analysis

The final step to post processing the PRISM data was visualization. In all the discussions that follow, "PRISM with Plasmasphere" or PSTECP are the PRISM runs made with the full OVTEC input (no data excluded), "PRISM without Plasmasphere" or PSTECO are PRISM run with the OVTEC below the latitude cutoff excluded, and "PRISM without Input (Climatology or PIM)" or PSTECC are model runs without OVTEC data input. OSTEC refers to the observed STEC.

PSTECP, PSTECO, PSTECC, and OSTEC files were plotted directly as a function of IPP local time to determine the quality of GPS calibrations and PRISM model runs. PSTECP, PSTECO, and PSTECC files were then compared to OSTEC and plotted as functions of elevation angle, horizontal grid location, and local time. PSTECP was then compared to PSTECO and also plotted as function of elevation, horizontal grid, and local time. Finally, the distribution bin files and statistics were plotted in histograms both by individual data day, and as a summary of all data days.

4. Summary and Analysis

GPS Data Availability

With only two exceptions, every day of data requested was available. Factors other than availability limited the actual days selected. The exact set selected was based on the 10-per-season impetus stated in previous sections, and is shown in Table 2.

Table 2: GPS File Inventory.

Index	Data	Data Day	Data Date	Index	Data	Data Day	Data Date
1	1997	070	03/11	21	1998	259	09/16
2	1997	071	03/12	22	1998	260	09/17
3	1997	072	03/13	23	1998	262	09/19
4	1997	073	03/14	24	1998	263	09/20
5	1997	075	03/16	25	1998	264	09/21
6	1997	076	03/17	26	1998	265	09/22
7	1997	077	03/18	27	1998	267	09/24
8	1997	078	03/19	28	1998	268	09/25
9	1997	081	03/22	29	1998	269	09/26
10	1997	082	03/23	30	1998	270	09/27
11	1997	170	06/19	31	1999	005	01/05
12	1997	172	06/21	32	1999	006	01/06
13	1997	173	06/22	33	1999	007	01/07
14	1997	174	06/23	34	1999	008	01/08
15	1997	175	06/24	35	1999	009	01/09
16	1997	176	06/25	36	1999	010	01/10
17	1997	177	06/26	37	1999	012	01/12
18	1997	178	06/27	38	1999	014	01/14
19	1997	179	06/28	39	1999	015	01/15
20	1997	180	06/29	40	1999	016	01/16

SCORE Results

Only two files were found to be unusable due to availability. The receiver at Pittsburgh on day 171, 1997 was inoperable from 23:19 to 23:59 UT [Drosdak, 1999]. This made that data incomplete, and a different day was selected in its place. Also, data provided in the

1999, day 011 data set were found to actually contain values from 1999, day 009. The cause of this was undetermined, but this also led to selection of a different day. Other data gaps were due to effects such as anomalous bias or orphaned GPS calibration discussed below.

Some orphaned GPS calibrations occurred during the SCORE (see Section 2.1.5) process when there was insufficient latitude intersection of compared samples. Figure 16 shows an example for data on day 080, 1997. Here, an IPP database with calibrated Equivalent VTEC is plotted as a function of IPP Local Time. Also, the lower portion shows the IPP latitude position of the GPS. When there's no intersection of latitudes, the SCORE process is unable to resolve a bias value for that satellite. The result is un-calibrated satellite passes or orphans, and the whole data set is compromised. In all, three files fell victim to this; 1997 days 074 and 079, and 1998 day 261.
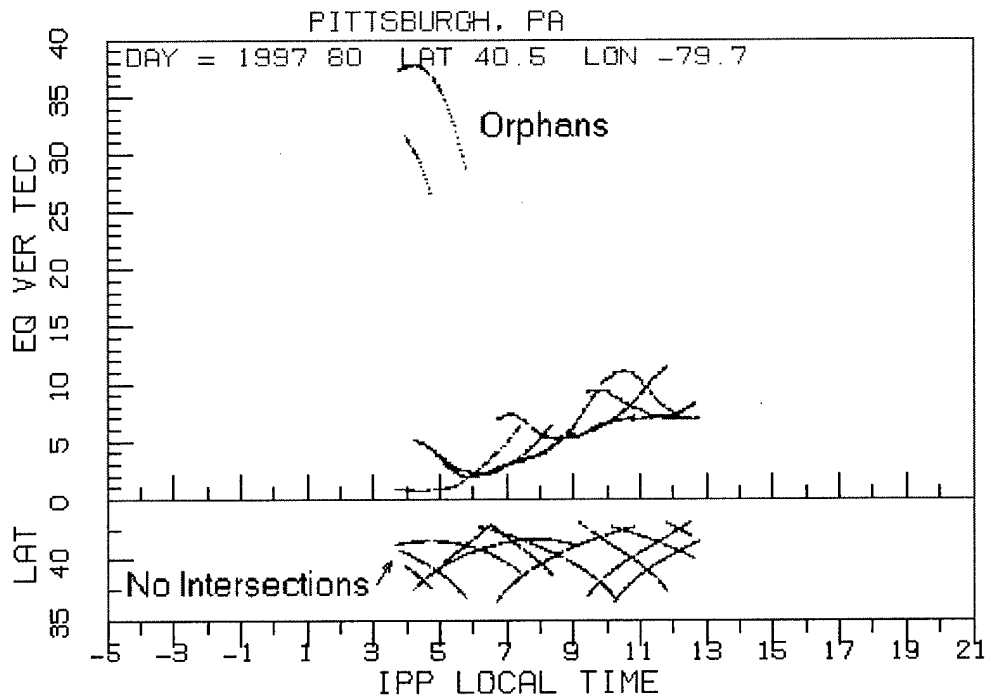
Figure 16: Orphaned GPS Measurement.

Anomalous bias constituted the second issue, and this had two different effects.

Anomalous bias occurred when the data recorded by the satellite was significantly different

than expected. For a given day, each satellite should have a relatively constant bias value

for each of its passes. The receiver at Pittsburgh has been known to infrequently inject a

phase shift which shows up as additional bias in the measure [Mazzella, 1999]. An

example is for 1998 day 261 shown in Figure 17.
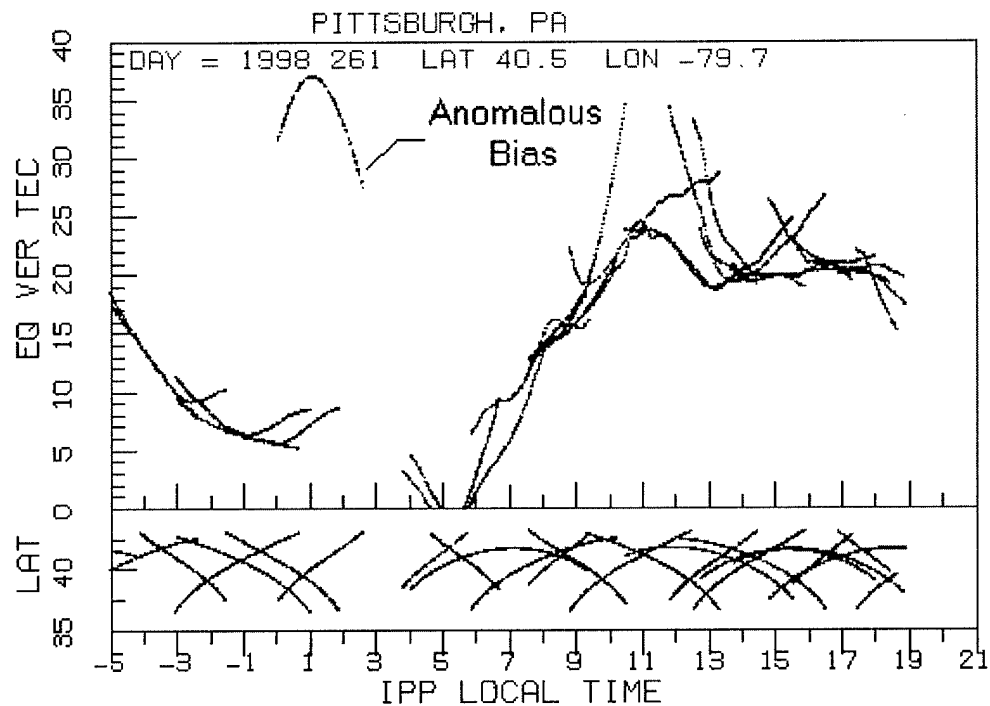
Figure 17: Anomalous Bias.

Along with the failure to properly calibrate the individual satellite pass, the bias values

determined for passes immediately prior to and after are incorrectly shifted. Nominal

values for TEC at −1 IPP local time are on the order of 2 TECu. Here, bias values bring the

measurement only down to 5 TECu. Also, a bias value should never adjust a measurement

to read a negative TEC as can be seen at approximately 5 IPP local time. Six days were

affected by this phenomena; 1997 day 072, 1998 days 266, 267, 269, and 270, and 1999 day 013.

Though not effective in every case, a work-around was employed to modify the bias levels of some of the data set. During solar quiet periods, receiver and antenna bias values should not vary significantly on adjacent days [Mazzella, 1999]. Using this, the bias levels for adjacent days were applied to the anomalous set. For 1997 day 072, and 1998 days 267, 269, and 270, biases were applied from day 071, 268, 271, and 271 respectively.

GPS to PRISM Input Conversion

A total of 11,520 PRISM input files were produced using the thin shell approximation discussed in Section 3.1.5, the IPP window shown in Figure 13: User Friendly 9-point Grid, and a sample rate of 15 minutes. Each individual OVTEC PRISM input data file contained approximately 5-7 data points. Once the additional constraint of latitude cutoff was employed to produce PRISM input without plasmaspheric distortion (PSTECO), that number fell to approximately 3. The climatological runs required no input data. Table 3 shows an example PRISM input for 1997, day 072, hour 23, minute 45, where plasmasphere is included. All times in this input file are between 23:45 and 24:00, IPP latitudes less than 43.55° and greater than 37.55°, and IPP longitudes less than −75.2° and greater than −84.2°. Equivalent VTEC is the value calculated by the thin shell approximation equation, and the comment block simply refers to the type of data, and latitude/longitude southeast corner. PRISM specifies the entire PRISM grid discussed in Section 0 using these 5 input points.

Table 3: Sample PRISM Input File.

Year	Day	UT	IPP Latitude	IPP Longitude	Equivalent VTEC	Comment
1997	72	2349	40.79	-80.4	6.3	IMS+40-079
1997	72	2349	44.4	-85.59	6.2	IMS+40-079
1997	72	2350	40.78	-77.16	4.8	IMS+40-079
1997	72	2350	41.55	-75.74	6.3	IMS+40-079
1997	72	2349	39.28	-83.51	7.8	IMS+40-079

PRISM Auxiliary Inputs

4.1.1. Within The Observational Window

All auxiliary inputs for the entire data set were available without exception. Figure 18 contains the IMF parameter B_z, and K_p plotted for the 1998 data set. An interesting feature occurs in the area of 09/25/98. Here, the solar activity is such that a value for K_p on the order of 9, and a large and rapid shift in B_z occurs. A similar event of lesser magnitude (not shown) occurs on 06/27/97 with K_p's reaching 4.8.
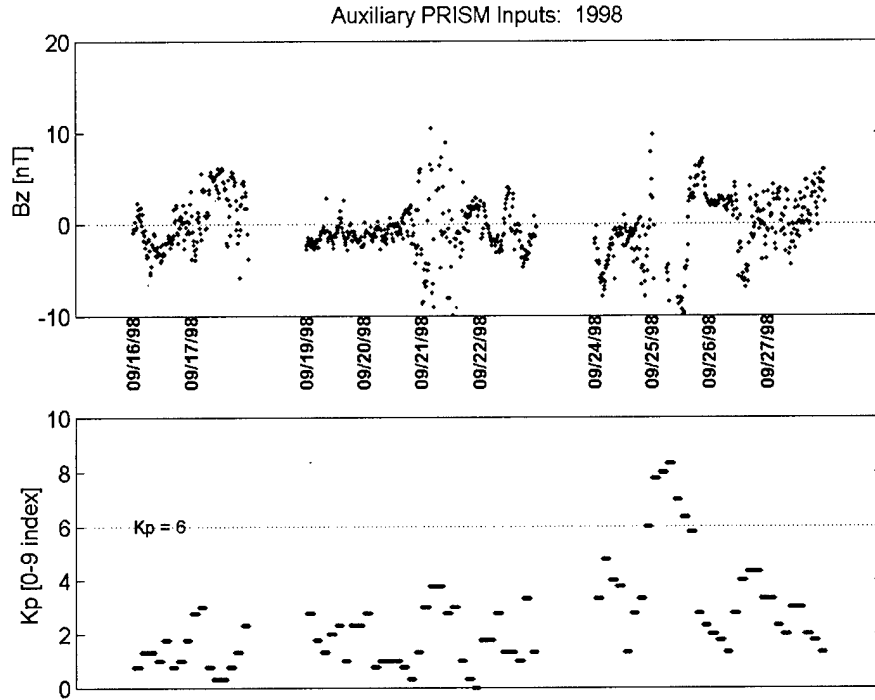
Figure 18: PRISM Auxiliary Inputs for 1998.

4.1.2. Upstream Auxilliary Inputs

Along with GPS calibration, another important feature affecting the PRISM executions

was the geomagnetic activity upstream of the selected data day. Plasmaspheric response to

the onset of geomagnetic storms is to immediate depletion of the plasmasphere by

tangential stress, or drag [Kivelson and Russell, 1995]. This depletion is followed by a

much slower filling from the underlying ionosphere. Time scales on the order of 16 days

are considered sufficient to fully allow the ionosphere to back-fill the plasmasphere [Lunt

et al., 1999]. So, this investigation had to account for periods beyond 12-16 days of a

geomagnetic storm. With a K_p of 6 or greater considered unacceptably high, all of the data

days except the period after 1998, day 265 were acceptable.

The nearest time-span of concern aside from the 1998 days was the 1997 day 170+ period. Figure 19 shows K_p for 1997 plotted by day of the year. On day 160, a spike of 7.33 occurs with a second spike of 6.33 on day 178. With only 8 days allowed for the flux tubes to refill the plasmasphere, this epoch becomes questionable. It was allowed since the average time between geomagnetic storm-induced depletions is actually much shorter than 16 days [Kersley and Klobuchar, 1980], and the K_p of 6.33 just barely breached the 6.0 active level limit.
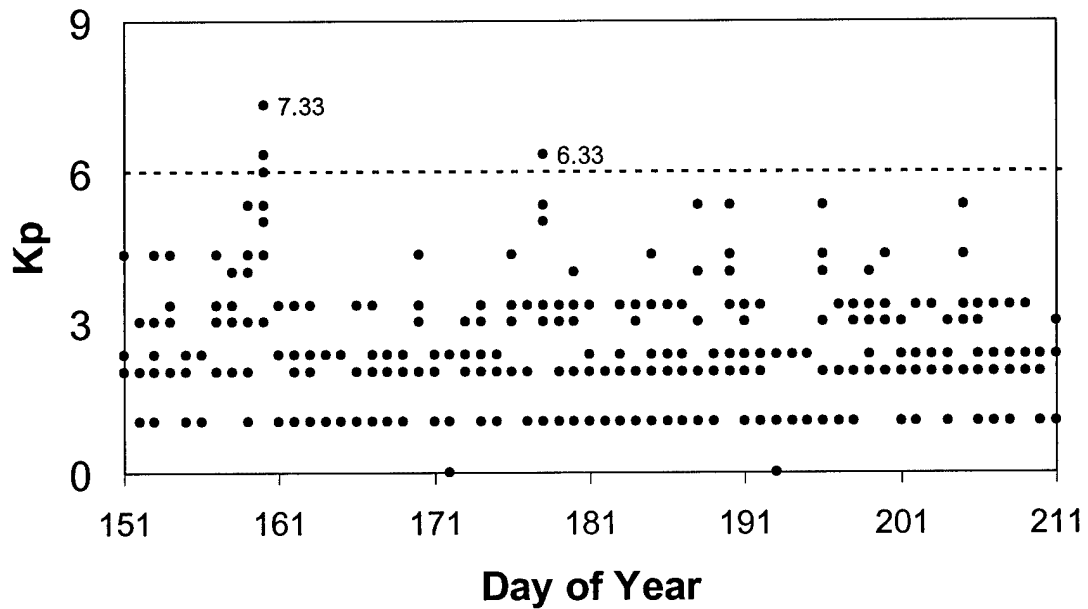
Figure 19: Kp for 1997.

PRISM Gridded Output to PSTEC

Reviewing the summaries of PSTECP, PSTECO, PSTECC, and OSTEC data plotted as a function of time revealed some consistent features. Figure 20 is an example of the STEC recorded for the overhead distribution bin (horizontal bin 5). This bin contains only STEC from IPP latitudes ranging from 39.55° - 41.55°, and longitudes from –81.2° to –78.2°.

This corresponds to elevations greater than 61°. Data collected from elevations above 61° are both less prone to plasmaspheric contributions and intersect less ionosphere along a LOS to the satellite. Distortions should be limited when taken in this nearly overhead bin. Refer to the figure for the discussion below.
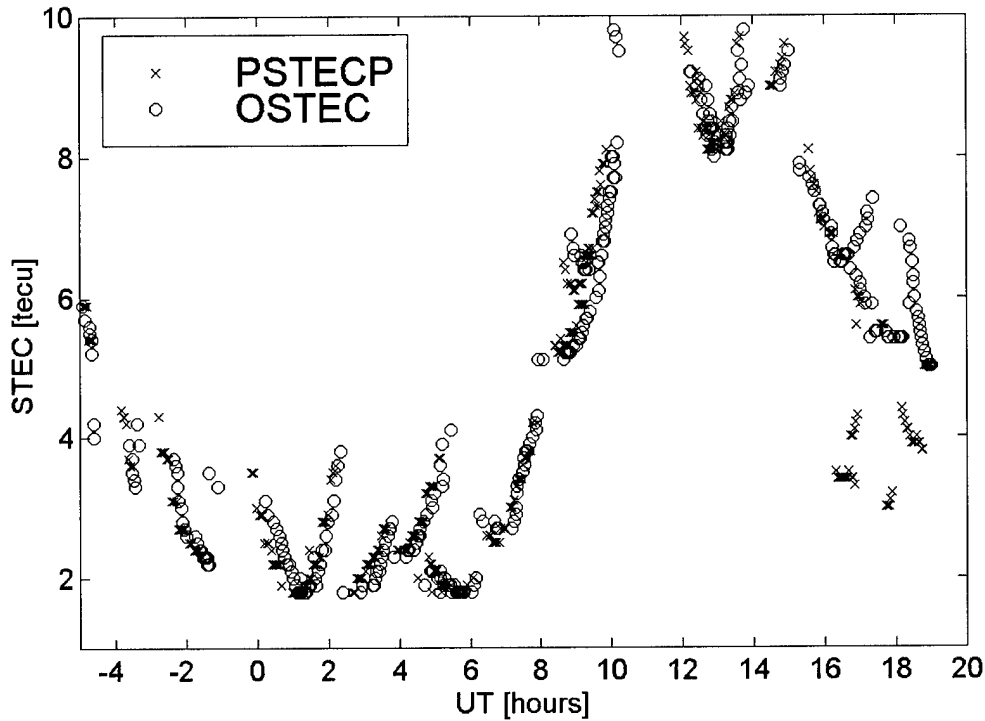
Figure 20: STEC Data Summary With Plasmaspheric Distortion, 1997, day 075.

PSTECP values coincide with the OSTEC closely in the time periods preceding mid-afternoon, but show disagreement on the order of 4 to 5 TECu after 16h. This feature appeared on nearly all data days sampled. Also, the influence of the trajectory of the GPS on the STEC is evident. For example, pick the data point at 0h and approximately 3.5 TECu, as time progresses, the plot traces out a continuous parabolic curve with a minimum value of 1.8 TECu, and a maximum of 4.0 TECu, terminating at approximately 2h. This represents a magnitude difference of 2.2 TECu, and corresponds to the trajectory of a GPS

acquired at the Pittsburgh site at a low elevation angle. In time, the GPS LOS proceeds

from that low elevation upward to a maximum value, then back down to a minimum

elevation. The STEC it measures will follow this trend since at the lower elevations, more

ionosphere is intercepted by the LOS. This trend in TEC was also seen previously in

Figure 17: Sample PRISM Input File. These general features were consistent throughout

PSTEC runs executed with and without the plasmaspheric distortion, but not as evident in

the climatology runs. This could be expected since there is no GPS input to PRISM in

climatology mode. Outputs in this case will not exhibit dependence on the GPS trajectory,

but will show variation due to STEC to VTEC conversion (see Section 3.1.5).

Along with the GPS elevation angle effect, there existed significant differences for the

climatological runs (PSTECC). Figure 21 summarizes such a PRISM execution with no

TEC input. Using only the physical models of PIM, PRISM's output is smoother, with no

evidence of the GPS trajectory-induced small-scale disturbances discussed above. Overall,

PSTECC overestimated OSTEC in each of the overhead cases. Overestimation ranged

from tenths of a TECu near 4h, to a maximum of 4 TECu at approximately 13h.
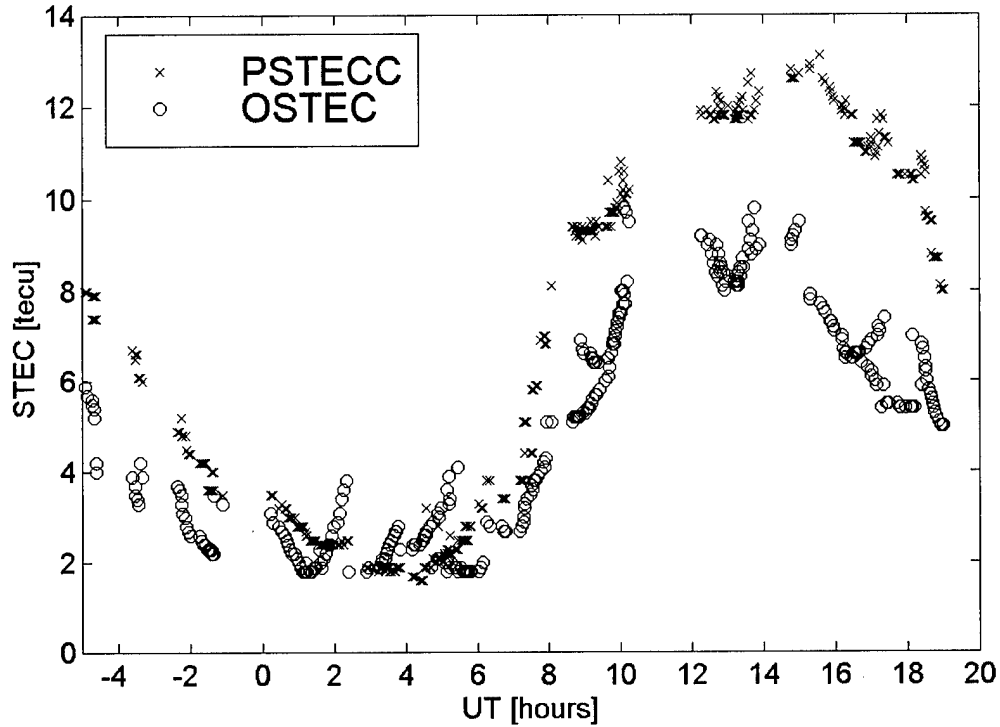
Figure 21: STEC Data Summary Climatology, 1997, day 075.

In response to the slow climb in solar activity, PRISM also produced higher STEC values later in the sample period. Figure 22 shows the same plot as in Figure 20, but for 1999 day 007. Immediately it can be seen that the OSTEC and PSTECP values are much higher than in 1997. Values of the order of 25 to 30 TECu were evident throughout 1999, with corresponding values for 1997 only reaching 10 to 12 TECu. The GPS trajectory-induced small-scale effect has a value of approximately 4.0 TECu, and the anomalous behavior after 16h (discussed previously) is evident for 1999 data.
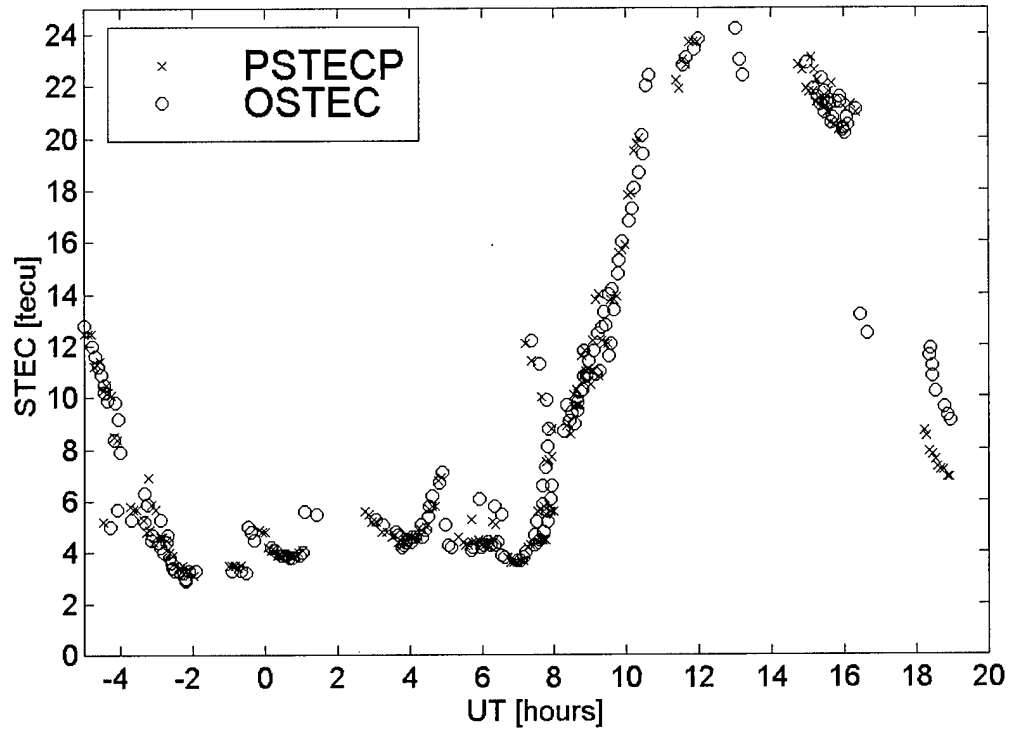
Figure 22: Data Summary with Plasmaspheric Distortion, 1999, day 007.

PSTECP and PSTECO Versus OSTEC

4.1.3. Elevation Comparisons

Figure 23 shows the ratio and difference between PSTECP and OSTEC for the same

1997 day 075, PRISM execution as a function of elevation angle. With little to no

observations taken below 34° elevation, it's impossible to make precise comparisons using

the regional application method discussed in Section 2.1.13, but over the range presented

here, the ratios and differences concur with the 0.965 and –0.85 TECu found in that limited

study (see Section 2.1.13). Here, at the lowest elevations, we can see small variations in

ratio on the order of 1.2, with differences ranging from –2 to 1 TECu (the data points near

the ratio of 0.5 and difference of –4.5 TECu are discussed in the following paragraph).

PSTECP values which follow closely the OSTEC was expected since the input includes the

maximum number of input data points in the PSTECP case. Fidelity should improve.

PRISM corrects all electron densities within the radius of influence (see Section 0) based

on weighted averaging of the input data [Daniell and Brown, 1995]. With the inclusion of

the lower latitude, protonospherically distorted input data, all the PRISM STEC

calculations within that region will be elevated.
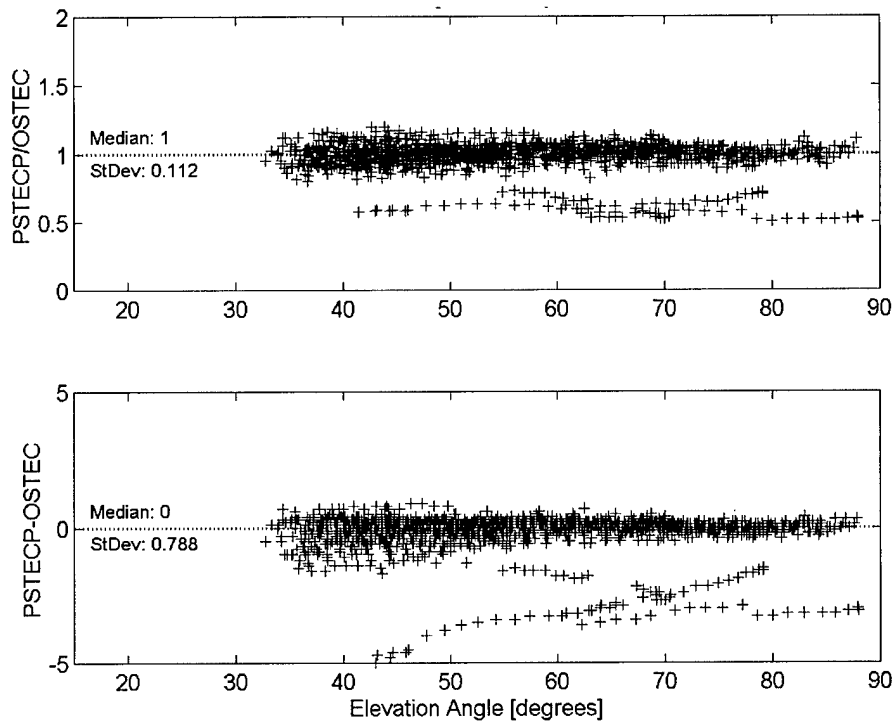
Figure 23: PRISM With No Data Excluded as a Function of Elevation, 1997 day 075.

The more significant differences on Figure 20 which occur at about 18 h, and on Figure

23 shown as a trace far removed from the median values, might be a result of dusk-induced

steep electron gradients. By inspecting the raw data files, it was found that the anomalous

values follow a single satellite observation recorded at approximately 18h. PRISM has

been shown to not respond accurately to steep gradients in ionospheric density [Coxwell,

1996 and Filby, 1997]. Scintillation events, equatorial anomalies, pre-reversal

enhancement, and dusk or dawn transitions can significantly increase the electron density

gradients and provide a challenge to PRISM. After 16h on Figure 20: STEC Data

Summary with Plasmasheric Distortion, there is a relatively sudden significant difference

between PSTECP and OSTEC which can be attributed to the dusk transition. By

individually selecting the data points from the elevation plot, it was found that the "off-

median" or spurious traces correspond to the near-dusk readings of the time plot. Since the

satellites pass from equator to pole relative to the Pittsburgh site, and the ionospheric

gradients at dusk are also longitudinally aligned, the STEC measured by a GPS would

remain within the steep gradient region throughout its pass. PSTEC will be modified by

the distorted observation, but will also be scaled down by adjacent OSTEC data, causing

the PSTEC output to be lower than observed.

In Figure 24, the entire collection of data values for PSTECP versus OSTEC were

plotted in bins from 18° to 90° with 2° elevation increments. The ratios are simply

PSTECP/OSTEC, and differences are PSTECP − OSTEC. The best ratios occur in the area

of 38° to 44° where they vary from 0.93 to 0.9. Differences in the same elevations range

are from −1.9 to −1.0 TECu. The next best correlations occur in the immediate vicinity of

46° with ratios falling off from 0.81 as elevation increases, and differences increasing in

magnitude from −2.1 TECu.
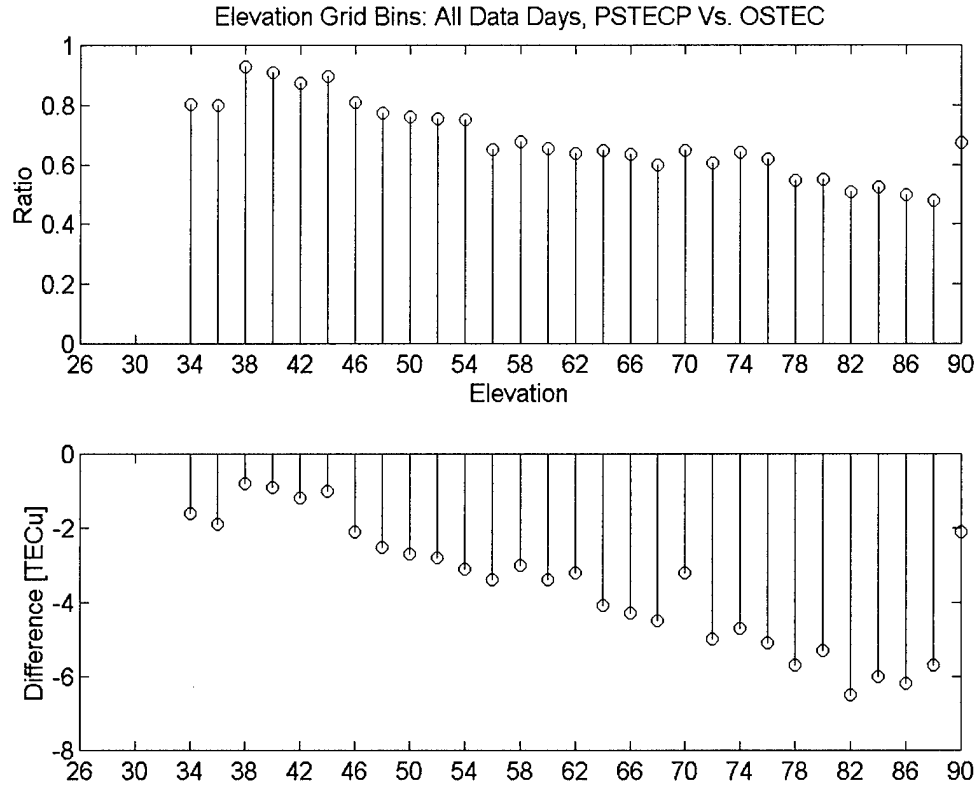
Figure 24: Elevation Bin Data Summary, PSTECP, All Data Days.

Measurements taken directly overhead (elevations near 90°) will be the most accurate

since they do not include horizontal gradient in the VTEC conversion. However, when the

elevation angle drops, more ionosphere is incorporated in the measurement, and the

disparity in TEC is expected to increase. Referring to Figure 11: Thin Shell

Approximation Comparison at 350 km, the thin shell approximate value is higher at the

lowest elevation angles when peering equatorward into plasmaspheric regions. This

approximated OVTEC is used to drive PRISM, and results in a slightly higher PSTEC

output than OSTEC. The ratios in this case are slightly higher for elevations below 78°.

The negative differences are consistent with an overall under-prediction of TEC by PRISM.

The PSTECO case is plotted as a function of elevation in Figure 25. The trends mirror that of the PSTECP case with one important difference. There is more variation at the lower elevations. This makes sense when considering the trajectory of the GPS. Without the additional plasmaspheric content below 40.75° IPP Latitude (which corresponds to approximately 83° elevation), those GPS traveling equatorward of this cutoff will be within the plasmasphere, and OSTEC will contain this additional TEC. However, others traveling at the same elevation, but poleward of the cutoff will continue to have the undistorted, good correspondence of the PSTECP case. Increases in the variability on the order of twice the PSTECP value can be expected with plasmaspheric contribution estimated at 2.5 TECu and low-elevation undistorted OSTEC on the order of 4 TECu. Here, standard deviation increases from the PSTECP case by a factor of 1.79 TECu.
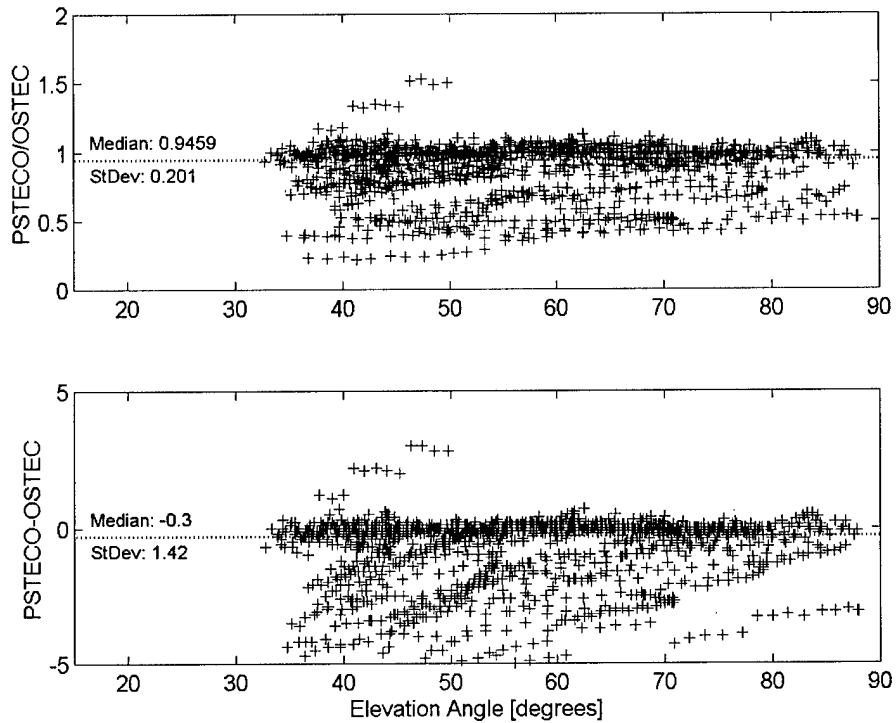
Figure 25: PRISM With Cutoff Data Excluded as a Function of Elevation, 1997 day 075.

Again, in Figure 26, the elevation grids have been plotted this time for the PSTECO versus OSTEC case. The best correlation occurs still in the area of 44°, with the spread of comparable ratios and differences ranging from 34° out to 78°. Differences are relatively constant with a maximum of –3 at 44°, and a maximum of –4.7 TECu at 36°. This comparison represents a sort of validation of PRISM output, where PSTECO values are compared with observation. And, it can be seen that PRISM has under-predicted TEC for 1997, day 075.
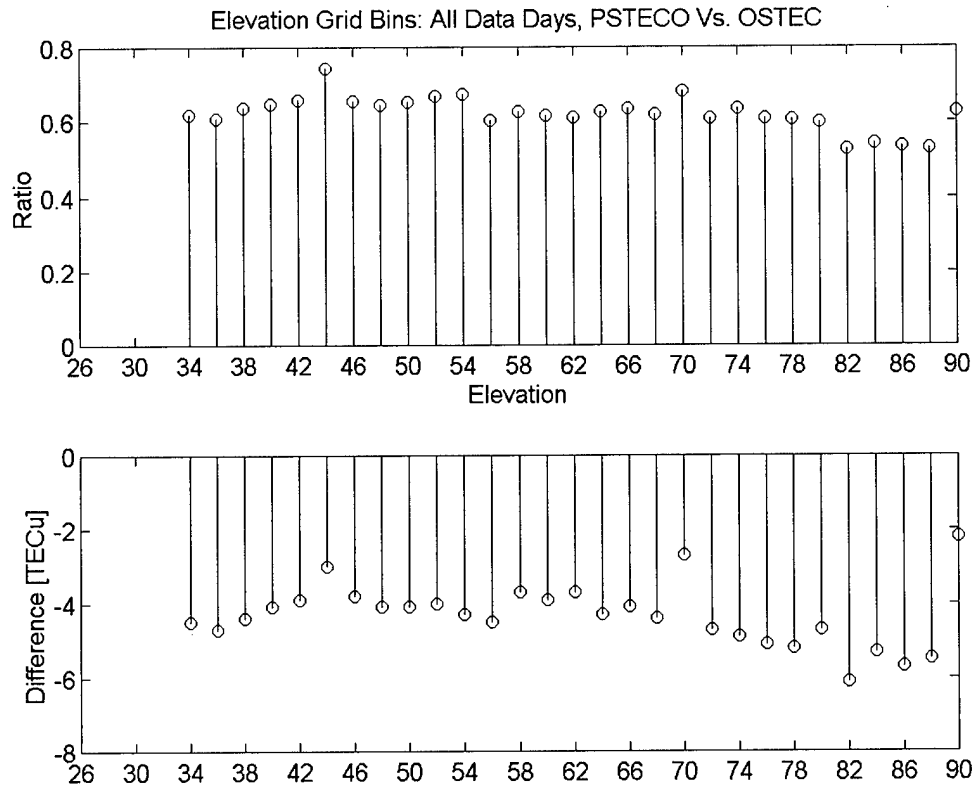
Figure 26: Elevation Bin Data Summary, PSTECO, All Data Days.

The third output in this regional test is the comparison of PRISM climatology (PSTECC) to OSTEC. An example of such a comparison is contained in Figure 27. Correlation between the two is poor. Visually, there is only a little evidence of a finely defined median, with data points spread widely about the mathematical median. Standard deviations for ratio and difference of 0.363 TECu and 2.19 TECu were large compared to the results for the PSTECP and PSTECO cases. This appears to contradict previous findings [Filby, 1997] where PRISM with GPS input was not able to specify TEC as well as PIM. The difference is in the calibration used on GPS TEC measurements. That study did not use SCORE, and the PSTECP calculated for that study was distorted by

protonospheric contributions. Now, with the improvement in GPS calibration, the PSTECP

values model the observations better than PIM alone.
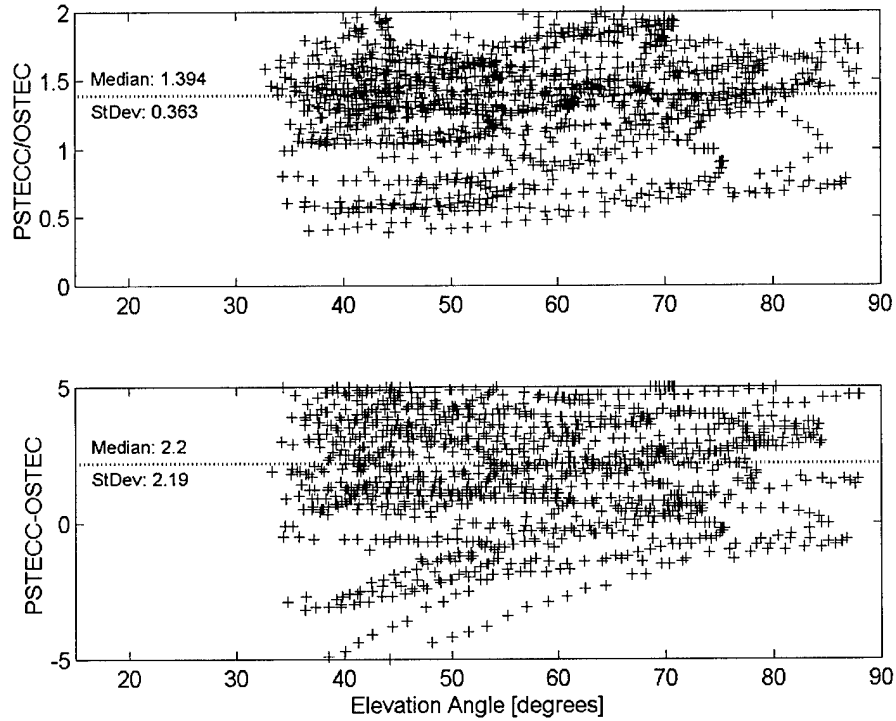
Figure 27: PRISM With No Data Input as a Function of Elevation, 1997 day 075.

4.1.4. 9 Point Grid

Another comparison for the PSTECP and PSTECO model runs was the 9-point

horizontal grid. The number of data points, ratios, and differences for all data days are

arranged in Table 4 in a grid laid out the same as the 9-pt horizontal grid (see Section 0).

For example, looking at the PSTECP case, there were 14,141 data points in the NW grid

(bin 7, see Figure 13), with a median ratio of 0.842, and a median difference of –2.20

TECu.

Table 4: Horizontal 9-point Grid Results for All Data Days.

all Days						PSTEC Vs. OSTEC		
Data Counts			Median Ratio			Median Difference		
PSTECP								
14141	33014	28957	0.842	0.711	0.695	-2.20	-3.10	-2.80
25071	55031	18998	0.889	0.574	0.665	-1.30	-5.20	-2.90
10239	35229	24340	0.920	0.691	0.771	-0.90	-2.80	-2.40
PSTECO								
14141	33014	28957	0.632	0.632	0.632	-5.00	-4.10	-3.70
25071	55031	18998	0.659	0.599	0.691	-3.90	-5.00	-2.40
10239	35229	24340	0.594	0.635	0.674	-4.80	-4.00	-3.70

PSTECP Standard Deviation from OSTEC					
Ratio			Difference		
0.704	0.507	0.504	10.25	9.83	10.39
0.560	0.379	0.315	9.94	9.21	7.36
0.541	0.478	0.552	10.95	9.75	10.47

PSTECO Standard Deviation from OSTEC					
Ratio			Difference		
0.568	0.462	0.442	9.85	9.53	9.93
0.477	0.430	0.396	10.02	9.36	7.80
0.423	0.438	0.468	10.85	9.55	9.86

Ratios for PSTECP ranged from 0.574 to 0.920, and for PSTECO from 0.594 to 0.691. Differences were from –5.2 to –0.9 TECu for PSTECP, and –5.0 to –2.4 TECu for PSTECO. When making a direct comparison of fidelity of the two cases, the overhead (center) bin is most appropriate choice since it will be least affected by environmental and geometric distortions. PSTECP has a slightly lower standard deviation in both ratio and difference than PSTECO case, suggesting a slightly higher degree of accuracy in the PSTECP case. The overhead bin was comparable to both the minimum ratios and maximum differences in both cases. Standard deviations for ratios ranged from 0.315 to 0.704 TECu with differences deviating from the mean by 7.36 to 10.95 TECu.

The data contained in Table 4 provides direct evidence that PRISM tends to under-predict STEC in the midlatitude regions (Pittsburgh is located in the North midlatitude

region of the globe). But, since the data set occurs during a time in which solar activity is steadily climbing and spans multiple seasons, it's not possible to say with certainty the amount of under-prediction that occurs. By calculating over the entire data set, the steady increase is included in the averaging, forcing the smaller early differences up, and the later time, greater magnitude differences, down. The table also includes the entire 40-day data set, which is distorted by the geomagnetic storm and recovery days at the end of the 1998 epoch.

Individual data days' contributions can be seen when each day is broken out and viewed as shown in Figure 28. Data days are displayed by index (see Table 2: GPS File Inventory, in Section 0).
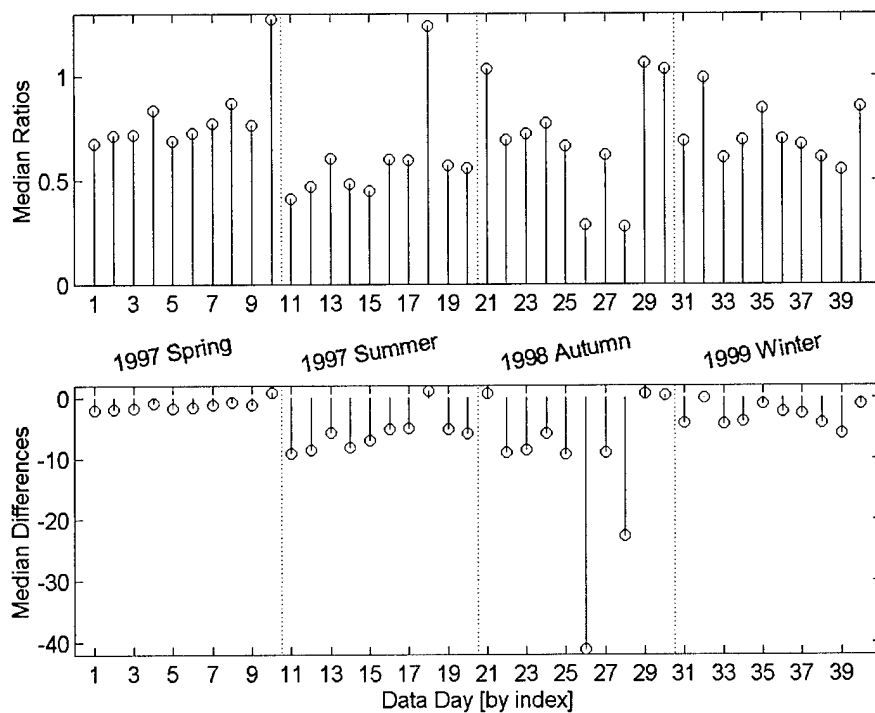
Figure 28: Overhead PSTECP Data Summarized by Day.

Large magnitude differences and corresponding small ratios occur on 1998 days 265 and 268 (index numbers 26 and 28). During this period, the significant magnetic storm activity discussed in Section 0 was in full force. Assumptions used in the VTEC conversion become suspect when the electron density profiles differ appreciably from nominal values.

Table 5 shows the same statistic developed for the data set excluding the storm and recovery days (day 1998, 265-270). A small change in ratios, and significant change in differences was seen. Ratios now ranged from 0.6 to 1.012, and differences from –4.6 to - 0.2 TECu. Even with the drastic values for the storm days of ratios on the order of 0.2 and differences as great as –40 TECu, relatively small changes in the summarized table could be expected since the entire data set included 245,020 data points, and the combined total for the five days excluded came to only 30,000 or 12.2%.

Table 5: Statistics Excluding Days 1998, 265-270.

	all Days excluding 1998, 265-270						PSTEC Vs. OSTEC		
	Data Counts			Median Ratio			Median Difference		
PSTECP	12470	29380	24580	0.866	0.733	0.726	-1.90	-2.80	-2.30
	21816	48712	17690	0.960	0.600	0.669	-0.40	-4.60	-2.70
	8314	31541	20517	1.012	0.745	0.809	0.20	-2.30	-1.90
PSTECO	12470	29380	24580	0.661	0.667	0.659	-4.50	-3.40	-3.00
	21816	48712	17690	0.703	0.616	0.707	-2.90	-4.30	-2.10
	8314	31541	20517	0.663	0.690	0.719	-3.00	-3.20	-3.00
PSTECC	12470	29380	923	0.575	0.661	0.647	-6.10	-4.30	-3.40
	21816	48712	17690	0.667	0.582	0.775	-3.95	-5.30	-1.90
	8314	31541	20517	0.662	0.644	0.676	-3.80	-3.80	-4.40

PSTECP Standard Deviation from OSTEC					
Ratio			Difference		
0.712	0.501	0.495	7.78	6.83	6.71
0.548	0.369	0.300	6.72	5.83	4.21
0.499	0.466	0.550	6.21	6.66	7.11

PSTECO Standard Deviation from OSTEC					
Ratio			Difference		
0.577	0.456	0.439	7.22	6.41	6.02
0.474	0.425	0.384	6.82	6.11	4.88
0.407	0.428	0.468	6.20	6.29	6.41

Though not shown here, similar analysis of individual data days was also accomplished, and aside from the magnetic storm days already discussed, there was little deviation from median ratios and differences.

4.1.5. Time

The same example day is now sorted in time, and plotted in Figure 29. Again, the overall correlation is very good with median ratios and differences very near 1 and 0 TECu respectively. The plot revealed again the significant departures of PSTECP from OSTEC during the dusk period from 16h to 18h, as well as some anomalous behavior at -2h, 4h, and 7h. The reasons for the elevations in ratio and difference in the hours prior to 16h are unknown. It has been suggested that anomalous satellite TEC measurements are the cause

[Mazzella, 1999]. This is plausible since the departures at –2h, 4h, and 7h follow a trend (not a random pattern), which suggests that the data has been taken from a single satellite and not a sample of several satellites. The feature from 16h to 18h, though not quantified in this study, is seen to exist at an approximate ratio of 0.95 and a difference of –2.5 to -5 TECu in each data day reviewed. It is likely to be associated with the dusk-induced steep ionospheric density gradients discussed previously in Section 4.1.3.
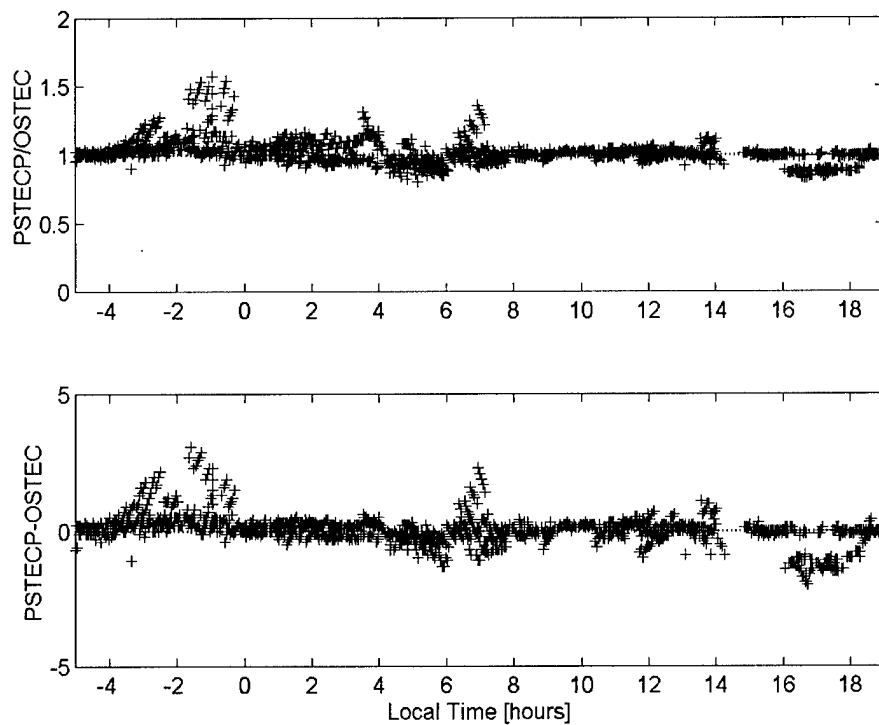
Figure 29: PSTECP Versus OSTEC as a Function of Time, 1997 day 075.

Protonospheric Quantitative Comparison

The real test for this study comes with the comparison of PSTECP and PSTECO. The effect of protonospheric contributions, evident in the ratios and differences of these two quantities, is summarized and presented below.

4.1.6. Elevation Comparisons

Day 1997, 075, PSTECP versus PSTECO is shown in Figure 30. There is far more

spread in the data values than previous samples when PSTECP was compared with

OSTEC. This is largely due to the substantial deviations associated with lower elevations.

The low elevation angle ratio datum includes both OVTEC within the plasmaspheric region

to the south and the protonosphere-free region poleward. As a result, ratios are more varied

at these elevations. As the LOS nears overhead, corresponding to elevation in the 80° to

90° range, the ratios become less varied and are centered at a value less than one.

Differences also show this same trend, with the greater variation at low elevation angles,

and less variation below zero as LOS approaches overhead.
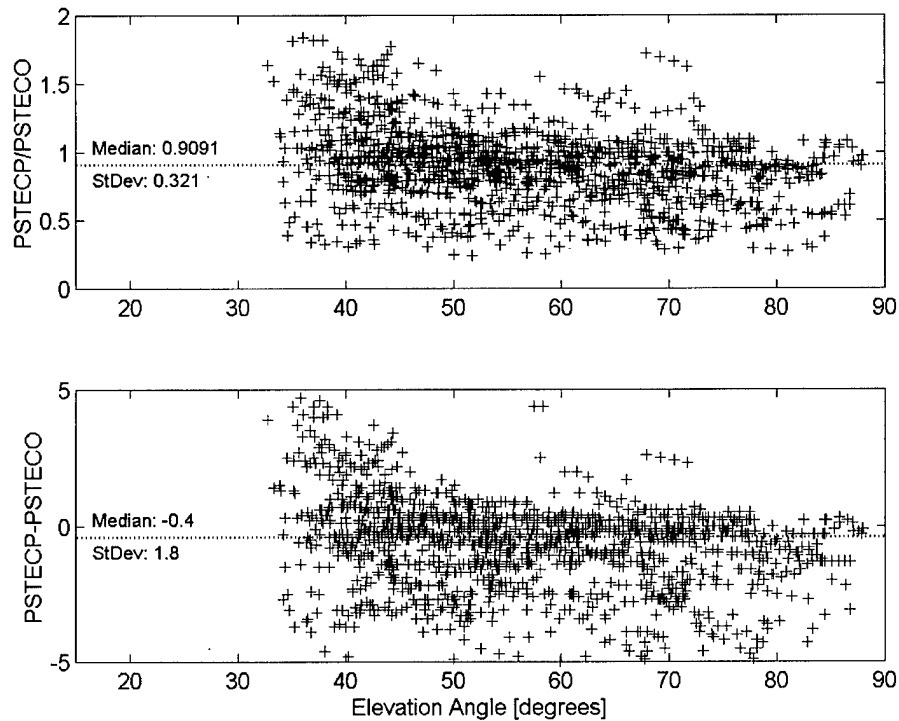
Figure 30: PRISM With and Without Plasmasphere as a Function of Elevation, 1997 day 075.

PSTECP values within the region below the latitude cutoff value, were expected to be higher than the PSTECO case since PSTECP includes the plasmaspheric contribution, and PSTECO does not. Consider a nominal plasmaspheric contribution of 2.5 TECu, and a PSTECO value of 0.5 TECu taken in a solar quiet period during the hours of darkness. PSTECP/PSTECO ratios in this case are 6. As time progresses into afternoon, TEC increases to values on the order of 20 TECu. The 2.5 TECu contribution results in a PSTECP/PSTECO value of 1.125 at the same elevation. The two-dimensional analysis here only considers one independent variable at a time. To make the distinction between elevations at different times, future plots would need to be binned by time as well (see Section 5.1.6).

Elevation comparisons for all the data days' PSTECP versus PSTECO are contained in Figure 31. Ratios are steadily above 1 up to an elevation of 62°, with the remainder falling very near 1. Unfortunately, the sample at the overhead point (90°) contains only 385 of a total of 245,020 points. This amounts to only 0.0016 of the total data points. By comparison, the maximum distribution in the 46° elevation bin contains 16,111 or 0.066 of the total. The result at the overhead point is less statistically significant than the other ratios. Future studies should include more data samples to improve the overhead point's statistical significance.
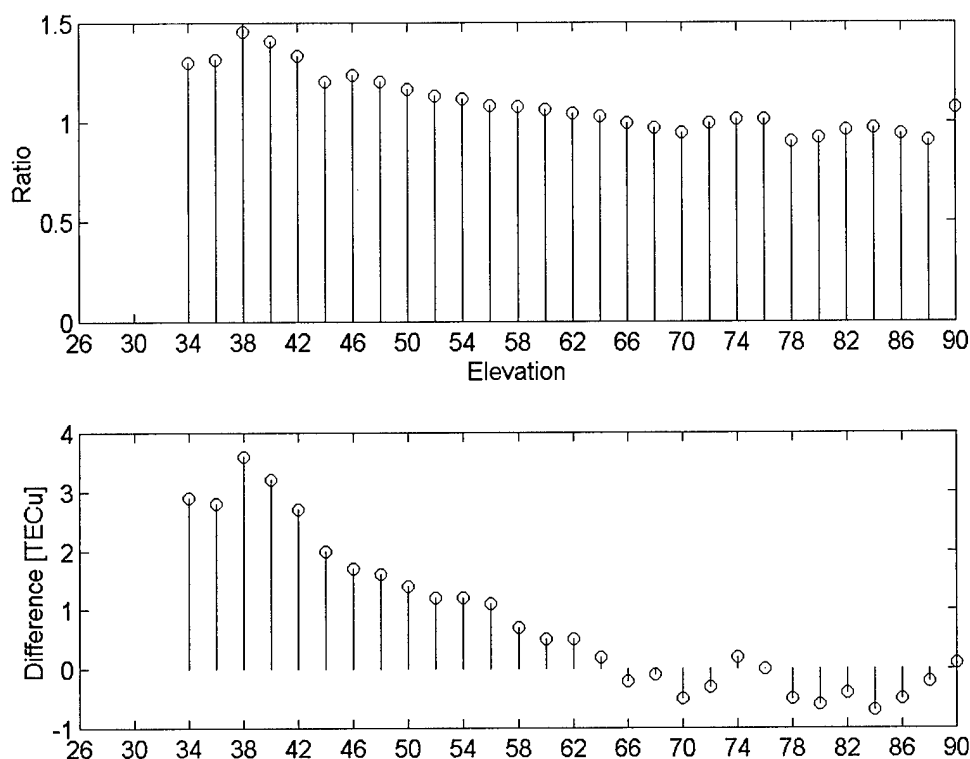
Figure 31: Elevation Bin Data Summary, PSTECP Vs. PSTECO, All Data Days.

Trends are the same as those found in the single day case. Values near 90° continue to be those that are least effected by the OSTEC to VTEC conversion, and are most representative of a direct comparison between PSTECP and PSTECO. To determine the protonospheric contribution to PRISM, elevations below 83° need to be separated in terms of those equatorward and poleward. This diagram does not do this, and therefore provides no direct values for plasmaspheric contribution. The horizontal grid comparisons made in the following sections does delineate between poleward and equatorward, thereby providing the separate values needed to make the protonospheric comparison.

When the storm and recovery days are removed, the results are modified slightly as shown in Figure 32. A variety of adjustments are made ranging from shifting the ratios at the 34° up by 0.1 to dropping many of the ratios above 78° by 0.03. Differences change the most at 34° with a drop of 0.8 TECu, but show very little change at regions very near overhead.
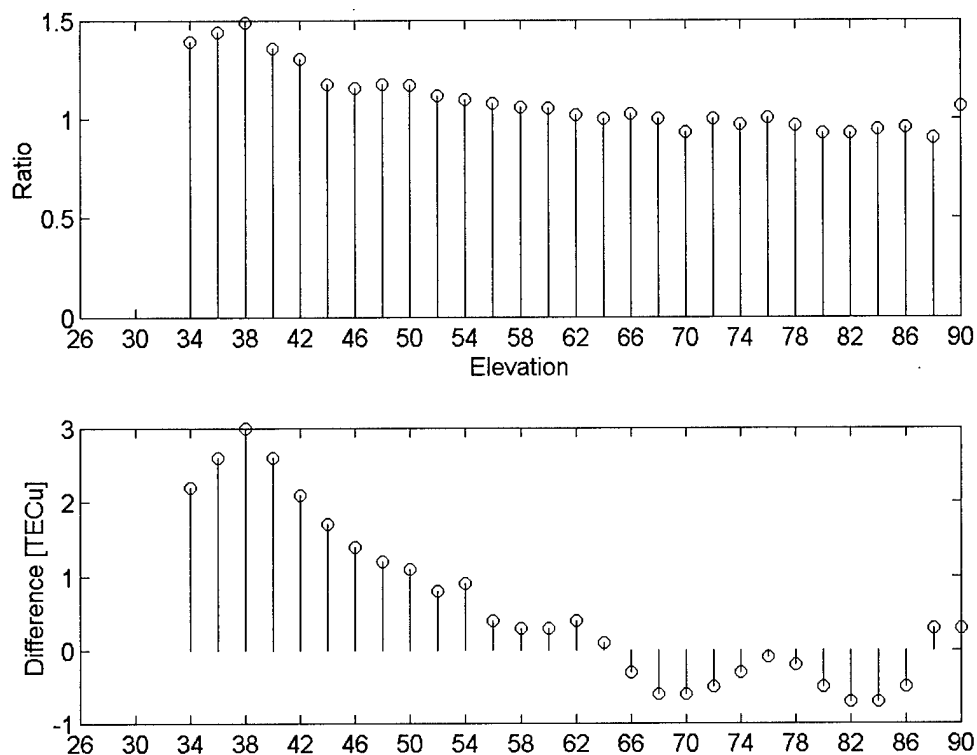
Figure 32: Elevation Bin Data Summary, PSTECP Vs. PSTECO, Storm and Recovery Days Excluded.

4.1.7. 9 Point Grid

Similar to the comparison methods used for PSTECP versus OSTEC, the statistical summary for 1997, day 075 is shown in Table 6. Ratios for PSTECP/PSTECO range from

0.858 to 1.827 while differences vary from -0.45 to 3.0 TECu. In both cases, bins 1, 2, 3,

and 4 (SW, S, SE, and W) exhibit the greatest magnitudes.

The south region differences are due to the plasmaspheric distortion from the

equatorward LOS. The quantity investigated in this study is the difference between

PSTECP and PSTECO. For the day in Table 6, the plasmaspheric contribution to PRISM

averages out among the southward bins to 1.93 TECu.

Table 6: Horizontal 9-point Grid Results for 1997, Day 075, PSTECP Vs.
PSTECO.

						PSTECP Vs. PSTECO		
Data Counts			Median Ratio			Median Difference		
214	260	162	0.964	1.221	1.047	-0.45	0.80	0.30
509	445	202	1.827	0.942	0.858	3.00	-0.10	-0.40
178	289	389	1.558	1.271	1.502	2.80	1.40	1.60

The large magnitude differences are not so easily characterized in the west (bins 1, 4,

and 7). One possible cause is due to the time the observations. Local time for the data

period begins and ends at 19h, meaning during fall and winter, Pittsburgh is 36 minutes

into darkness at the beginning of the sample. Dusk TEC enhancements are still settling,

and individual measurements made during this period tend to be noisy. In contrast, the east

region of the IPP grid is nearly an hour further into darkness at the beginning of the sample,

and ionospheric gradients are less steep. Variations at the eastern longitudes, at least

initially, are less likely to occur. As time passes for the data day, both the west region

settles then both the west and east regions experiences the full range of solar-induced

ionospheric enhancement at dawn, the peak TEC of mid-day, and the very unsettled period

about the pre-reversal enhancement and dusk. Comparisons of the two should be

consistent for overhead-aligned and eastern longitudes since they both experience the same range of TEC variation. The west will be more varied, however due to the settling time at the beginning of the data day.

Table 7 contains the statistics for PSTECP versus PSTECO for all data days in the study. Again, with the inclusion of the magnetic storm and recovery days, the PSTECP versus PSTECO comparisons are distorted. Ratios range from 0.957 to 1.548 and differences from –0.5 to 3.90 TECu. The greatest differences exist in the south and west regions. The plasmaspheric contribution contained in the south region results averages out to 2.13 TECu. When the western longitudes are removed from the comparisons, the average protonospheric contribution becomes 1.25 TECu.

Table 7: Data Summary for PSTECP Versus PSTECO, all Data Days.

						PSTECP Vs. PSTECO		
Data Counts			Median Ratio			Median Difference		
11017	11775	14272	1.333	1.124	1.101	2.80	1.00	0.90
15529	16111	10789	1.349	0.957	0.962	2.60	-0.20	-0.50
7673	10134	12878	1.548	1.088	1.144	3.90	1.20	1.30

Table 8 contains the same data as Table 7, excluding the magnetic storm and recovery days. In this case, the ratios become 0.946 to 1.525, and the differences range –0.6 to 3.2 TECu. The most varied regions in the study remain the south and west longitudes. When the west values are removed, ratios drop to a range of 0.946 to 1.125, with differences of – 0.6 to 1.1 TECu. Protonospheric contribution averages out to 1.73 TECu when all regions are included, and 1.0 TECu when only the south and east longitudes are considered. This

value represents the quantity of protonospheric contribution on PRISM output sought by

this study.

Table 8: Data Summary for PSTECP Versus PSTECO, all Data Days excluding 1998 Days 265-270.

								PSTECP Vs. PSTECO
Data Counts			Median Ratio			Median Difference		
9541	10260	12512	1.310	1.099	1.101	2.60	0.60	0.70
13566	13842	9261	1.366	0.974	0.946	2.50	-0.30	-0.60
6604	8774	11264	1.525	1.080	1.125	3.20	0.90	1.10

5. Summary, Conclusions, and Recommendations

Summary

This study set out to quantify the effect of the protonosphere on PRISM version 1.7c using calibrated GPS TEC measurements. Forty days of GPS TEC data were initially calibrated using SCORE, with the final data set including 35 days. The calibrated data was then used as input to the model under three conditions; one containing all available GPS TEC data, the second free from protonospheric contribution with data below a 40.75° IPP latitude excluded, and the third under climatological conditions with no GPS TEC data. The protonospheric contribution was determined by comparing PRISM output under the "all data" condition with PRISM output under the "data excluded" condition.

Conclusions

5.1.1. GPS TEC Measurements and SCORE

Data availability and coverage were really quite good. Though only 35 days were used to make the final comparisons, 40 day were successfully calibrated. With only 46 days attempted, this failure rate amounted to 15%. And, of those 6 unusable days, only 2 were because of equipment failure or availability. If the calibration methods are improved to allow for successful correction of anomalous bias or orphaned measurements, this failure rate would have been actually 4.5%. The weakness with GPS TEC measurements is the variability as a function of satellite trajectory. Though OVTEC will vary as a function of horizontal TEC gradients, if the conversion from OSTEC to OVTEC were perfect, it should not vary with elevation angle. Errors due to horizontal TEC gradients and multipath effects make the OVTEC reported by GPS appear to be a function of elevation angle. Maximum variations in OVTEC were shown in Section 0 to be on the order of 4.0 TECu.

Also, the use of the SCORE process combined with the exclusion of plasmasphere through use of a latitude cutoff, has improved the fidelity of PRISM when using GPS TEC as input. The ratios and differences from the PSTECP versus OSTEC case were much better than corresponding values for the PSTECC versus OSTEC case. Since PSTECC is the same as running only the PIM portion of PRISM, this result can be compared to a previous study [Filby, 1997], where PRISM with GPS input was found not to specify TEC as well as PIM. Though not quantified here, PRISM fidelity has been markedly improved with the use of SCORE.

5.1.2. PRISM Using GPS TEC as Input

PRISM modeled TEC fairly well in the PSTECP case, reproducing nearly overhead STEC to within 2.1 to 4.5 TECu under non-geomagnetic storm conditions. Even with storm and recovery days included, PSTEC was within 5.2 TECu of observed values, or 10.4% when the maximum TEC measurements were as high as 50 TECu. On days when OSTEC was only on the order of 12 TECu, PSTEC still ranged from 0.9 to 2.05 TECu or 17%. This is the same order of accuracy found in previous validations [Daniell et al., 1995]. The trajectory related measurement errors discussed above account for between 58% and 100% of the error.

When the outputs were compared as a function of elevation angle, the best ratios of PSTECP versus OSTEC occur in the area of 38° to 44° where they vary from 0.93 to 0.9. Differences in this same region vary from −1.9 to −1.0 TECu.

5.1.3. Protonospheric Contribution to PRISM

The protonospheric contribution to PRISM during non-geomagnetic storm periods was found to be an average of 1.0 TECu. This quantity is the difference between PSTECP and

PSTECO averaged over the 35 non-storm days in the horizontal grid directly south and southeast of Pittsburgh. This is the most appropriate comparison in this case for two reasons. For one, PRISM does not respond effectively to geomagnetic storm and recovery conditions. As a result, 5 geomagnetic storm and recovery days were removed from the data set, leaving only 35 data days. Secondly, the enhancement of magnitude in the SW bin of the horizontal grid, forced elimination of that grid bin from the calculation of the average. Though not entirely understood, it's possible that dawn and dusk ionospheric gradients located at the beginning of the observation times, caused anomalous or noisy readings in the western regions (see Section 4.1.7).

Recommendations

5.1.4. GPS TEC Measurement and Calibration

GPS TEC continues to be an excellent source of ionospheric and protonospheric data, and the SCORE process calibrates these data to high degrees of accuracy. There are three areas where this data and the processes used to calibrate it could be improved.

One would use the protonosphere as part of the calibration. SCORE gains most of its accuracy by excluding OSTEC from latitudes that are known to include the plasmasphere. Depending on the latitude of the receiving station, this could limit the data available to accomplish the calibrations. For example, Charleston, S. C., uses a latitude cutoff of 33.1° N [Law, 1999]. This equates to an elevation angle of approximately 77.7°, which is a reduction of 6.4% from the acceptable elevation angle of 83° used in Pittsburgh.

Another improvement would find a method for including anomalous bias and/or orphaned measurements. Though not exactly a change to the calibration algorithms, this would avoid failures encountered in this and previous studies. Particularly important is the

case of anomalous bias where a single failure in a satellite pass causes the entire data set to be modified. A work-around includes simply excluding the offending satellite pass, but as always, deleting data does not serve the same purpose as recovering and using data.

A third improvement could adjust the time frame for the actual observation. as can be seen on Figure 33 below, GPS data is recorded from 19 UT to 19 UT. This leads to a relatively steep gradient in TEC both at the beginning of the observation period and at the end. Since the calibration begins where the previous days' ends, but does not include information from that previous day in the calibration, any small variability in that data point will be carried into the calculation for the current day. To improve continuity, it would be better to begin the observation during the quieter continuous region between –3h and 7h UT.
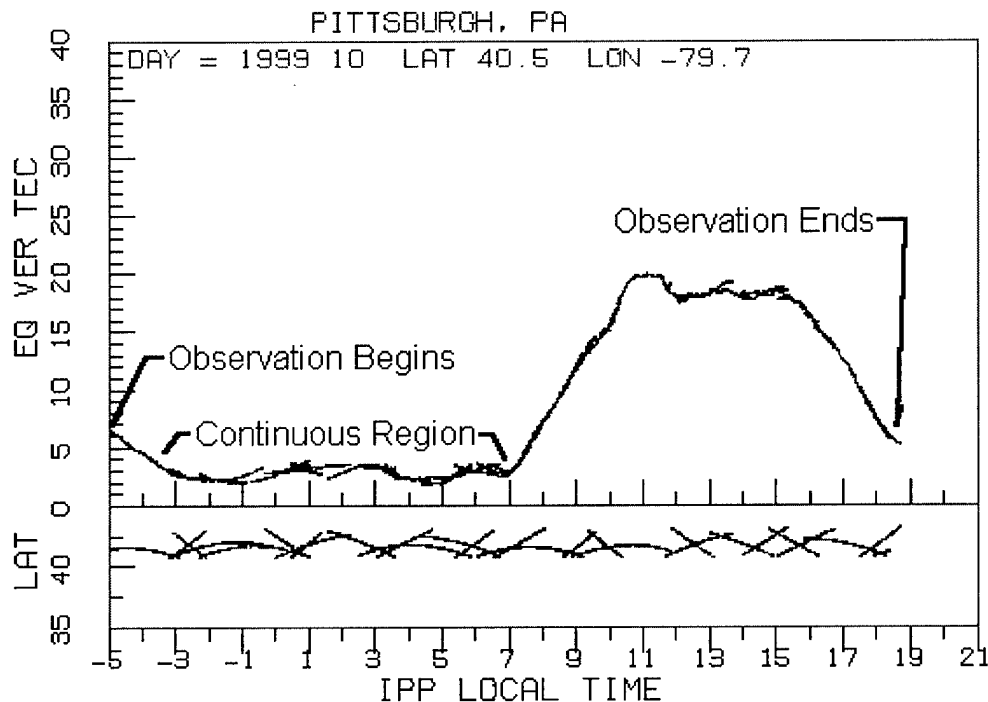
Figure 33: Smoothed VTEC for 1999, day 010.

76

5.1.5. PRISM

PRISM continues to be a good method for characterizing the ionosphere. Model results expressed above show maximum errors of 10.4% - 17% when compared to observed values, but the model is currently limited to altitudes of 1600 km and less. This includes what is considered the ionosphere, but leaves out any ionic content above the 1600 km. A physical model for the toroidal region above that altitude would allow proper specification particularly in the plasmaspherically involved regions extending from 60° N. to 60° S. latitude.

PRISM is also limited in its ability to handle geomagnetic storm periods, and regions of steep gradient such as the pre-reversal enhancement near dusk. The median difference on the worst of geomagnetic storm days was in excess of –40 TECu indicating a strong inability to respond to extremely dynamic conditions. Also, in response to the steep gradients found during dusk and dawn periods, comparison differences were fully twice that in quieter regions.

5.1.6. Future Studies of PRISM using GPS TEC as Input

A limited set of conclusions came from the methods used in this study, constrained by the following questions that serve to provide a framework for future study:

- How do the horizontal grids respond to time, and is the dusk effect as pronounced as it appears in this study? Though the horizontal grid provided some idea of protonospheric contribution, time proved to be a considerable factor. Previous studies [Coxwell, 1996] made strides in this direction, but used observations from a limited source just over the oceans to validate PRISM response to the dusk-induced ionospheric gradients. Future efforts could extend both that previous work, and

77

expand on the database provided here by further separating the horizontal bins into local time bins as well. For example, values in the overhead bin 5 could be parsed out as a function of local time, providing a critical view of dawn and dusk periods as well as diurnal TEC variations. This could be done with the current data set used here since GPS time is available in both the raw and calibrated databases, or more data could be compiled following the methods described in Appendix C: Data File Manipulations.

- How does the increase in solar activity affect the comparisons made here? There was an increase seen in the OSTEC, but since the horizontal bins were not plotted as a function of time, this time-dependant variation could not be extracted. Also, the data here spanned all four seasons, which have their own response to the sun. And, by compiling the data as was done here, comparison across seasons was not possible. Analysis could be done on the current data set, or again, more data from the same season could be brought together from different years to analyze this effect.

- Are the results of this study consistent within the hemisphere, or just a feature of Pittsburgh? This study could be expanded to include multiple locations, thereby including more geographic locations at or near the same latitude. This would lead to more data needed to quantify the protonospheric effect.

As a final word, though GPS receiver antenna bias calibration methods have been improved, and the magnitude and contributions of the protonosphere are better understood, any investigator or operator must be aware of the limitations and strengths of using GPS data with PRISM. Careful calibration of GPS TEC is effective in over 85% of all cases studied here, but the results when converted to PRISM input are still heavily affected by elevation angle and time of day. PRISM outputs calculated from nearly overhead GPS measurements are the most accurate. Also, PRISM responds poorly to geomagnetic storm and recovery conditions. Though normally accurate in TEC output to within 10 – 17%, error as high as 100% can be induced by large or rapid variations in the ionosphere such as in storms or along the dawn to dusk terminator.

Appendix A: GPS Bias Calibrations (SCORE)

Specific details on the algorithms used in SCORE are contained in the report on ionospheric TEC investigations [Andreasen et al., 1998]. Here, a brief technical overview has been provided.

A.1. The Error Equation

The calibration is a minimization of correlated measurement discrepancies where one receiver records data from several different satellites. The minimization is defined below in Equation A.11 [Bishop et al., 1994].

$$E = \tfrac{1}{2} \sum_\alpha \sum_i^{I\alpha} \sum_{\beta \neq \alpha} \sum_j^{J\beta} W_{\alpha i,\beta j} \times (T_{\alpha i} - T_{\beta j})^2 \tag{A.11}$$

where,

$\alpha i = i^{th}$ sample of satellite α

$\beta j = j^{th}$ sample of satellite β

$W_{\alpha i,\beta j}$ = weighting factor between samples αi and βj

T = VTEC calculated for sample αi and βj

Equivalent VTEC is the same as discussed in Section 3.1.5, with a slight modification to allow for satellite bias minimization, and shown again in Equation A.12 below.

$$VTEC = (S_{\alpha i} - B_\alpha) \left(\cos(\sin^{-1}(\frac{R_e}{R_e + IPPAlt} \cdot \cos(El))) \right) \tag{A.12}$$

where,

$S_{\alpha i}$ is the uncorrected STEC for the data sample

B_α is the combined receiver and satellite bias, in TECu, for satellite α

A.2. Weighting Factors

The weighting factor $W_{\alpha I, \beta j}$ treats the measurements from a pair of satellites using a number of factors; IPP latitude, IPP local time, universal time, and elevation angle. When the samples differ by large amounts in any of these factors, their correlation is low. Therefore, their weighting factor is small. The formulation of $W_{\alpha I, \beta j}$ is shown in Equation A.13 below.

$$W_{\alpha i, \beta j} = \exp(-\frac{1}{2}(\frac{\theta_{\alpha i} - \theta_{\beta j}}{\theta_0})^2) \times \exp(-\frac{1}{2}(\frac{\lambda_{\alpha i} - \lambda_{\beta j}}{\lambda_0})^2) \times \exp(-\frac{1}{2}(\frac{\tau_{\alpha i} - \tau_{\beta j}}{\tau_0})^2) \times \sin^n(\varepsilon_{\alpha i}) \times \sin^n(\varepsilon_{\beta j}) \quad \text{(A.13)}$$

where the subscripts are the same as before with the exception of 0 which indicates a reference value used for controlling the scaling,

θ = IPP latitude for the data sample

λ = IPP local time for the data sample

τ = universal time for the data sample

ε = the elevation angle for the data sample

n = exponent for elevation weighting

For example, $\theta_{\alpha i}$ is the ith IPP latitude for satellite α. And $T_{\beta j}$ is the jth universal time value for satellite β.

A.3. Bias Calculation

The actual calculation of bias for a single satellite is done by taking the first derivative of the Error equation (A.6) with respect to each of the B_α values, setting the solutions to zero, then solving the linear system for each B_α.

Appendix B: Receiver Independent Exchange Format Version 2.0

B.1. ASCII File Types

The data files are available in four ASCII file types; the observation data, navigation message, meteorological data, and GLObal NAvigation Satellite System (GLONASS) data. The only file used here is the observation data file.

Filenames followed two conventions depending on whether it was recorded prior to December 1997. Files prior to that date were compiled every 5 seconds, and were recorded with each hour's data in separate files. After December 1997, the sample rate changed to 30 seconds, and whole day's data was compiled into a single file. Each hourly file was named as SSSSDDDF.YYo where SSSS specifies the station ID, DDD is the three-digit julian day, F is an alphabetical character indicating the hour (e.g., a for 00h, b for 01h, etc.), and YY is the two-digit year. For the daily files, F is simply not included in the filename. For example, pit1078b.97o is the filename for the pit1 site, day 078, hour 01, in 1997, and pit1010.99o is for day 010, all hours, in 1999.

B.2. Header Record Information

The RINEX-2 file is basically composed of two parts; the record header and the observational data. Information contained in the record header includes site ID, receiver and antenna location and type, comments about the conditions of observation, and number and types of observations. When the data was collected under anti-spoofing conditions (as discussed in section 3.1.3), a comment was placed in the header.

B.3. Observables

RINEX-2 files for Pittsburgh contain only 6 observable data. This data is tabulated under the headings C1, L1, L2, P1, P2, D1, and D2. Specific details of each can be found

in the paper by Gurtner [1997]. What's important for this study are the values contained in the C1, L1, L2, and P2 columns. C1 contains the pseudorange on frequency L1 calculated using the Coarse/Acquisition (C/A) signal code. P2 has the same pseudorange but for L2 using the less noisy Precise (P) code. L1 and L2 are the measures of relative phase difference on each signal. Since this site is under the anti-spoofing conditions (see section 3.1.3), data under P1 is not available.

Appendix C: Data File Manipulations

C.1. GPS Data

The manipulation of files leading up to and including the final calibration using SCORE is shown below in step-wise fashion. Each of the algorithms used is listed in sequence with an example of the command line, and a small explanation below it.

C.1.1. GETNOAA.BAT pit1 99 010 kelly.doser

Here, *pit1* indicates the site, *99* the two-digit year, *010* the three-digit julian day, and *kelly.doser* the email address for FTP anonymous access.

All data used in this study were readily available from National Geodetic Survey (NGS) web site www.ngs.noaa.gov/CORS. All of the data prior to December 1997 had to be individually requested via email, but the remainder was immediately available through the web page. For the email requests, a message was sent with the particular days, site, and hours of the request. Then, they would put the requested data on a specified directory for subsequent download through FTP. All of the data arrives in compressed format.

C.1.2. NOAAPASS.BAT pit1 99 010 0 x

All inputs are the same as above with *0* indicating a daily file (the case for all files after 97), and the *x* specifying AS correction needed.

NOAAPASS first decompresses the data files, joins files as needed, then executes RINMTI to calculate STEC. Data was stored at the NOAA web site compressed using GZIP. Each days data was then held in one of two formats; hourly and daily. The hourly formats were reserved for data prior to 1998, with daily files thereafter.

Daily file naming conventions followed PIT1dddo.gz where *ddd* was the julian day, *o* indicated an observational file, and *gz* represents the files was compressed using GZIP.

Once decompressed, the file becomes PIT1ddd0.yyo where the *0* is immediately removed by NOAAPASS. The final filename is PIT1ddd.yyo used in the TEC calculation executable RINMTI.

Hourly file naming conventions followed PIT1dddh.yoz, where *ddd* held the julian day, *h* the alpha character representing the hour of the day, *y* the one-digit year, *o* indicating the files is an observation file, and *z* the character indicating the file was compressed. Once uncompressed, the file becomes PIT1dddh.yyo. NOAAPASS then joins all the hours in a single file using the same naming convention as the daily file for use again in RINMTI.

RINMTI calculates STEC and RNX2PAS4 produces an output pass file for each satellite using the naming convention ydddhhmm.pnn where *yddd* is the year and julian day, *hhmm* the hour and minute, *p* a character indicating pass file output, and *nn* the satellite identifier.

C.1.3. REPLSCHR 9010 p

RINMTI output includes the *p* character in the 10th position, but the following programs needed a 0 in that there. REPLSCHR swaps that character for all pass files on the current directory. Here, *9010* is the year and julian day, and *p* is the character to replace.

C.1.4. WPCKSTD 9010

WPCKSTD executes a standard deviation test on all the data and throws out any values with too great a variance from the mean. This file returns files named ydddhhmm.wnn.

C.1.5 FXJPSTD 9010

The carrier phase delay measurement is not an absolute measurement. The actual phase can vary depending on when the signal is first acquired. If the signal is lost even momentarily, the phase can be re-acquired at a different value. To maintain a constant

measurement of phase throughout the pass, it is usually necessary to realign the reacquired signal phase. FXJPSTD adjusts the phase measurement to maintain a smooth measurement throughout the pass. Output from FXJPSTD are named ydddhhmm.fnn.

C.1.6. REPLSCHR 9010 0 p

To keep from overwriting the original pass files, their 10th character is replaced with a p.

C.1.7. REPLSCHR 9010 f 0

For use in subsequent programs, FXJPSTD output files are renamed replacing the 10th character with 0.

C.1.8. PEXAM 9010

The final step to preparing the files for calibration is visual examination. Here, an added step has been introduced using a Mathcad algorithm to further reduce "wild-points." This algorithm used a mobbing average within the data set, then eliminated data points within the window of that moving average that were outside 1.2 standard deviations.

PEXAM uses the new filename with the 0 10th character, and modify it's contents overwriting the same file.

C.1.9. GENAZEL 9004 9004 9011 9

Once the pass file data has been processed, azimuth and elevation information was produced using almanac files from the "Yuma" link contained on the gpstest.46tg.af.mil/webpub/general/BBS.inf Air Force web site.

Here, 9004 is the year and julian day of the almanac file and the starting day for the azimuth/elevation file, 9011 is the ending day, and 9 is the first digit in the two-digit year.

The file output is named yddd.alm, and is used in subsequent processes.

C.1.10 RUNBCO 9 010 9004 40.75

RUNBCO executes the SCORE calibration. Here, *9* is the first digit of the two-digit year, *010* the julian day, *9004* the year and julian day of the azimuth/elevation file to use, and *40.75* is the latitude cutoff used.

Output files include log files, tables which include the biases and error estimates, and the IPP databases which are binary files with all the STEC data tabulated by azimuth/elevation at the 350 km ionosphere altitude.

All files produced to this point were placed in the ..\pit1\9010\ directory.

C.1.11. ALLI2PSM 9 010 9010

For use in PRISM, STEC from the IPP databases is extracted and converted to an equivalent VTEC in 15-minute bins throughout the day. Here, *9* is the first digit of the two-digit year, and *010* the julian day. Output files are named ydddhhmm.psm using the same conventions as above. Each file produced was placed in a new directory ..\pit1\9010\prismp\.

C.1.12. PSME.BAT 9010 40.75

To produce files not including plasmaspheric distortion, all data below the 40.75 latitude were excluded. PSME extracted all data above this cutoff and wrote the new files to the directory ..\pit1\9010\prismo\.

A third directory was created called ..\pit1\9010\prismc\ that held climatological PRISM manipulations.

C.1.13. RUNASTEC 9010

To facilitate comparison of OSTEC with values calculated by PRISM, the IPP database is converted to OSTEC. RUNASTEC converts all the IPP database files to OSTEC with the output files named stecyddd.nn.

C.2. PRISM Files

For each data day, under each of the input conditions (with and without plasmaspheric distortion and climatology), and at each 15-minute time interval (96 in all for a single day), PRISM was executed followed by the PRISM post-processor. The post-processor integrated along LOS to calculate PSTEC.

C.2.1. BIGBANG.BAT 9010

BIGBANG executed PRISM and the post-processor for each of the three conditions for each time interval over an entire day. Output files include the log file ydddhhmm.log, the post-processor output file ydddhhmm.tec, and the PRISM control file ydddhhmm.in.

The actual gridded output files from PRISM were deleted in the process due to their huge size. A single output file weighed in at over 9 Mb. With 288 files run for each day, and 40 days of data, the total just for these output files would have been over 250 Gb!

C.2.2. FIXISTEC 9010

FIXISTEC adds gps time to the PSTEC produced by the post-processor.

C.3. Statistics

After the calibration and production stages, the output data was arranged in bins according to both the horizontal grid and elevation angles. After these extractions, several statistical values were calculated and recorded.

C.3.1. IBINS

IBINS is an executable used to open individual data days' yddd.tec output file, extract the bins according to both the horizontal grid and elevations, then write the extracted data to bin files under the ..\pit1\yddd\analysis\ directory.

The filenames used followed the convention binxx_px.dat where xx is the bin number, and px is the run-type (pp is with distortion, po is without, and pc is climatology). The bin numbers were assigned 00-09 for the horizontal grid, 34-90 for elevations.

IBINS also calculates and writes the statistical values to the file stats_px.dat, under the \analysis\ directory.

C.3.2. ABINS

ABINS accomplished the same but for all days. Output files were written to the ..\pit1\analysis\ directory.

C.3.3. 38BINS

Once the magnetic storm periods were discovered for days 8265 and 8268, statistics were re-accomplished excluding those days. 38BINS does the same as ABINS without these days. Output files from this process were named 38ats_px.dat.

Bibliography

American Institute of Aeronautics and Astronautics. Global Positioning System: Theory and Applications Volume I: Ed. Bradford T. Parkinson. Progress in Astronautics and Aeronautics, Volume 163, 1996.

Anderson, D. N., "*A Theoretical Study of the Ionospheric F-region Equatorial Anomaly, II, Results in the American and Asian Sectors,*" Planetary Space Science, 21: 421-442, 1973.

Andreasen, C. C., E. J. Fremouw, A. J. Mazzella, G. S. Rao, and J. A. Secan, "*Further Investigations of Ionospheric Total Electron Content and Scintillation Effects on Transionospheric Radiowave Propagation,*" Contract F19628-94-C-0067, AFRL-VS-HA-TR-98-0037. Bellevue, WA: Northwest Research Associates, Inc., 1998.

Bishop, G. D., R. Daniell, T. Bullett, S. Rao, A. Mazzella, and T. Denny, "*An application of PRISM to Regional Ionospheric Specification,*" Report to Air Force Research Laboratory, Space Vehicles Directorate, Hanscom AFB, MA, 1999.

Bishop, G., D. Walsh, P. Daly, A. Mazzella, and E. Holland, "*Analysis of the Temporal Stability of GPS and GLONASS Group DelayCorrection Terms Seen in Various Sets of Ionospheric Delay Data,*" Proceedings of ION GPS-94, The Institute of Navigation, Washington, D.C., 1994.

Brace, l. H., and R. R. Theis, "*Global Empirical Models of Ionospheric Electron Temperature in the Upper F-Region and Plasmasphere Based on in Situ Measurements from the Atmosphere Explorer-C, ISIS 1, and ISIS 2 Satellites,*" Journal of Atmospheric and Terrestrial Physics, 43: 1317, 1981.

Coxwell, D. R., Validation of the Parameterized Real-Time Ionospheric Specification Model (PRISM) Version 1.6B Using TOPEX Total Electron Content (TEC) Data, MS Thesis, AFIT/GAP/ENP/96D-05. School of Engineering, Air Force Institute of Technology (AU), Wright-Patterson AFB, OH, March 1996.

Daniell, R. E. Jr., and L. D. Brown, PRISM: A Parameterized Real-Time Ionospheric Specification model, Version 1.5, Contract F19628-92-C-0044, PL-TR-95-2061. Waltham, MA: Computational Physics, Inc., 1995(AD-A299664).

Davis, R. E., "*Predictability of Sea Surface Temperature and Sea Level Pressure Anomalies Over the North Pacific Ocean,*" Journal of Physical Oceanography, 6: 249, 1976.

Drosdak, J. "*Readme.171,*" Personal Communications, September 1999.

Fejer, B. G., "*The Equatorial Ionospheric Electric Fields, A Review,*" Journal of Atmospheric and Terrestrial Physics, 43: 377-386, 1981.

Fejer, B. G., E. R. De Paula, I. S. Batista, E. Bonelli, and R. F. Woodman, *"Equatorial F Region Vertical Plasma Drifts During Solar Maxima,"* Journal of Geophysical Research, 94: 12049-12054, 1989.

Fejer, B. G., E. R. de Paula, R. A. Heelis, and W. B. Hanson, *"Global equatorial ionospheric vertical plasma drifts measured by the AE-E Satellite,"* Journal of Geophysical Research, 100: 5769-5776, 1995.

Filby, S. D., A Validation of the Parameterized Real-Time Ionospheric Specification Model (PRISM) Version 1.7B, MS Thesis, AFIT/GAP/ENP/97D-03. School of Engineering, Air Force Institute of Technology (AU), Wright-Patterson AFB, OH, March 1997.

Gurtner, W., *"RINEX: The Receiver Independent Exchange Format Version 2,"* CSTG BPS Bulletin, (Revised), 1997.

Hardy, D. A., M. S. Gussenhoven, R. R. Raistrick, and W. J. McNeil, *"Statistical and Functional Representations of the Pattern of Auroral Energy Flux, Number Flux, and Conductivity,"* Journal of Geophysical Research, 92: 12275-12294, 1987.

Hedin, A. E., *"Empirical Global Model of Upper Thermosphere Winds Based on Atmospheric and Dynamics Explorer Satellite Data,"* Journal of Geophysical Research, 93: 9959-9978, 1988.

Heppner, J. P., and N. C. Maynard, *"Empirical High-Latitude Electric Field Models,"* Journal of Geophysical Research, 92: 4467-4489, 1987.

Jasperse, J. R., *"The Photoelectron Distribution Function in the Terrestrial Ionosphere,"* in Physics of Space Plasmas. Ed. Chang, T. S., Coppi, B., Jasperse, J. R., Scientific Publishers, Cambridge, MA: 53-84, 1982.

Johnson, C. Y., *"Ion and Neutral Composition of the Ionosphere,"* Annals of the IQSY, 5: 197-213, 1969.

Johnson, R. *"The Earth's Plasmasphere,"* Excerpt from Windows to the Universe, Regents of the University of Michigan, n. pag. WWWeb, http://www.windows.umich.edu/, 1999.

Kersley, L., and J. A. Klobuchar, *"Storm Associated Protonospheric Depletion and Recovery,"* Planet Space Sciences, 28: 453-458, 1980

Kivelson, M. G., and C. T. Russell, Introduction to Space Physics, Cambridge University Press, Cambridge, 1995.

Kutzbach, J. E., *"Empirical Eigenvectors of Sea-Level Pressure, Surface Temperature, and Precipitation Complexes over North America,"* Journal of Applied Meteorology, 6: 791, 1967.

Law, K. M., <u>Validation of the Gallagher Protonospheric Model</u>, MS Thesis, AFIT/GAP/ENP/99M-04. School of Engineering, Air Force Institute of Technology (AU), Wright-Patterson AFB, OH, March 1999.

Lorenz, E. N., <u>Empirical Orthogonal Functions and Statistical Weather Prediction</u>, Contract AF19(604)1566, AFCRC-TN-57-256, Department of Meteorology, MIT, 1956.

Lunt, N., L. Kersley, G. J. Bishop, A. J. Mazella, and G. J. Bailey, *"The Effect of the Protonosphere on the Estimation of GPS TEC: Validation Using Model Simulations,"* <u>Radio Science, 34</u>: 1261-1271 1999.

Mazzella, A. J., Personal Communications, September, 1999.

Peixota, J. P., and A. H. Oort, <u>Physics of Climate</u> (Appendix B), American Institute of Physics, New York, 1991.

Rees, M. H., <u>Physics and Chemistry of the Upper Atmosphere</u>, Cambridge University Press, Cambridge, 1989.

Schunk, R. W., *"A Mathematical Model of the Middle and High Latitude Ionosphere,"* <u>Pure Applied Physics, 127</u>: 255-303, 1988.

Strickland, D. J., D. L. Book, T. P. Coffey, and J. A. Fedder, *"Transport Equation Techniques for the Deposition of Auroral Electrons,"* <u>Journal of Geophysical Research, 81</u>: 2755-2764, 1976.

Strickland, D. J., R. E. Daniell, J. R. Jasperse, and B. Basu, *"Transport-Theoretic Model for the Electron-Proton-Hydrogen Atom Aurora: 2. Model Results, in Press,"* <u>Journal of Geophysical Research</u>: 1994.

Wells, D. E., N. Beck, D. Delikaraoglou, A. Kleusberg, E. J. Krakiwsky, G. Lachapelle, R. B. Langley, M. Nakiboglu, K. P. Schwarz, J. M. Tranquilla and P. Vaníček, <u>Guide to GPS Positioning</u>," Fredricton, N. B., Canada: University of New Brunswick Graphic Services, 1986.

Xiaoqing, P., *"Real-Time Ionospheric Total Electron Content (TEC) over North America (Space Weather Campaign - Sept 1999),"* Excerpt from <u>Ionospheric and Atmoshperic Remote Sensing</u>, Jet Propulsion Laboratory, n. pag. WWWeb <u>http://sideshow.jpl.nasa.gov/gpsiono/latest.html</u>, 1999.

<u>Vita</u>

Captain Kelly Doser was born 31 December, 1963 in Seattle, Washington. He received an Associates Degree in Electronics Technology from the Community College of the Air Force in 1995, a Bachelor of Science in Electrical Engineering and a Bachelor of Science in Atmospheric Sciences from the University of Washington in 1997. He enlisted in the United States Air Force on June 15, 1984, and was commissioned a second lieutenant on 22 September, 1997, then promoted to captain in 1999.

He's been assigned to several locations including Keesler Air Force Base, Mississippi; Lindsey Air Station, West Germany; Brooks Air Force Base, Texas; Yokota Air Base, Japan; Air Force Reserve Officer Training Corps. Detachment 910, Washington; and Ansbach Army Heliport, Germany before coming to the School of Engineering and Management, Air Force Institute of Technology, Wright-Patterson Air Force Base, Ohio in August 1998.

Permanent Address: 17420 58th Street SE
Snohomish, WA 98290

REPORT DOCUMENTATION PAGE		Form Approved OMB No. 074-0188
Public reporting burden for this collection of information is estimated to average 1 hour per response, including the time for reviewing instructions, searching existing data sources, gathering and maintaining the data needed, and completing and reviewing the collection of information. Send comments regarding this burden estimate or any other aspect of the collection of information, including suggestions for reducing this burden to Washington Headquarters Services, Directorate for Information Operations and Reports, 1215 Jefferson Davis Highway, Suite 1204, Arlington, VA 22202-4302, and to the Office of Management and Budget, Paperwork Reduction Project (0704-0188), Washington, DC 20503		

1. AGENCY USE ONLY (Leave blank)	2. REPORT DATE March 2000	3. REPORT TYPE AND DATES COVERED Master's Thesis	

4. TITLE AND SUBTITLE QUANTIFYING THE PROTONOSPHERIC EFFECT ON PRISM	5. FUNDING NUMBERS
6. AUTHOR(S) Kelly B. Doser, Captain, USAF	

7. PERFORMING ORGANIZATION NAMES(S) AND ADDRESS(S) Air Force Institute of Technology Graduate School of Engineering and Management (AFIT/EN) 2950 P Street, Building 640 WPAFB OH 45433-7765	8. PERFORMING ORGANIZATION REPORT NUMBER AFIT/GAP/ENP/00M-02

9. SPONSORING / MONITORING AGENCY NAME(S) AND ADDRESS(ES) AFRL/VSBP Attn: Mr. Gregory Bishop 1865 4th Street Hanscom AFB, MA 01731 DSN: 785-3036	10. SPONSORING / MONITORING AGENCY REPORT NUMBER

11. SUPPLEMENTARY NOTES

Prof. W. F. Bailey, ENP, DSN 785-3636, ext.

12a. DISTRIBUTION / AVAILABILITY STATEMENT APPROVED FOR PUBLIC RELEASE; DISTRIBUTION UNLIMITED.	12b. DISTRIBUTION CODE

ABSTRACT (Maximum 200 Words)

There is a continuing effort to model the ionosphere accurately. One such approach, the Parameterized Regional Ionospheric Specification Model (PRISM) does so without considering ionic content above an altitude of 1600 km. Plasma exists, however, above this altitude in a region called the protonosphere, and has been shown to account for up to 50% of total electron content (TEC) measurements. The actual TEC contributed to a PRISM calculation has been studied using protonospheric TEC measurements made by Global Positioning Satellites (GPS). The challenges of including the protonosphere affect both the calibration of GPS measurements and execution of PRISM. Calibration of 40 days of GPS measurements over Pittsburgh, PA, revealed an average protonospheric contribution in the midlatitude regions of 2.5 to 3.0 TEC units (TECu). When used as input, these elevated measurements led to average PRISM outputs elevated by 1.0 TECu.

14. SUBJECT TERMS Meeting Management, Delphi Technique, Malcolm Baldridge, Business Meetings, Management, Leadership Training, Organizational Meetings, Quality, Meeting Guide, Meeting Training, Management Training, Organizational Theory, Group Dynamics			15. NUMBER OF PAGES 107
			16. PRICE CODE

17. SECURITY CLASSIFICATION OF REPORT UNCLASSIFIED	18. SECURITY CLASSIFICATION OF THIS PAGE UNCLASSIFIED	19. SECURITY CLASSIFICATION OF ABSTRACT UNCLASSIFIED	20. LIMITATION OF ABSTRACT UL

NSN 7540-01-280-5500

Standard Form 298 (Rev. 2-89)
Prescribed by ANSI Std. Z39-18
298-102